JCI The Journal of Clinical Investigation

Acetaldehyde dehydrogenase 2 interactions with LDLR and AMPK regulate foam cell formation

Shanshan Zhong, … , Yun-Cheng Wu, Huiyong Yin

J Clin Invest. 2018. https://doi.org/10.1172/JCI122064.

Research In-Press Preview Cell biology Metabolism

Graphical abstract

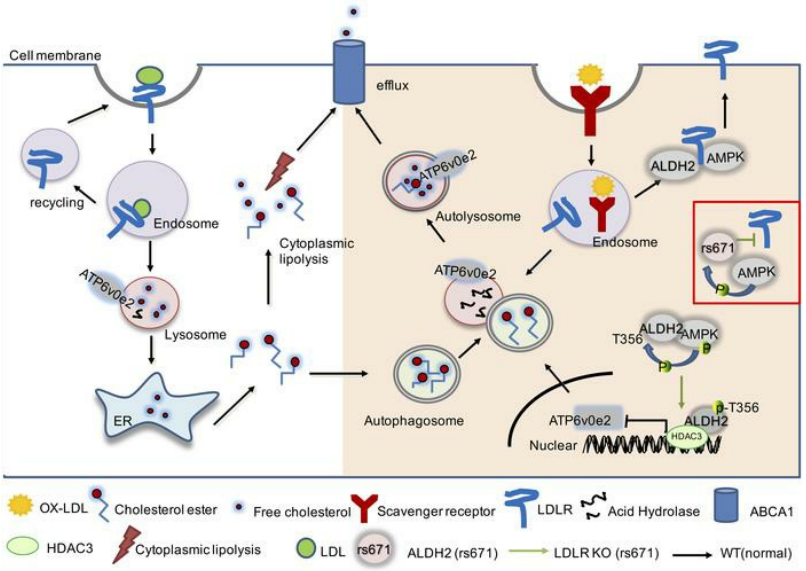

Find the latest version:

https://jci.me/122064/pdf

Acetaldehyde Dehydrogenase 2 Interactions with LDLR and AMPK Regulate Foam Cell Formation

Shanshan Zhong[1,2]; Luxiao Li[1,2,3]; Yu-Lei Zhang[4], Lili Zhang[1,2]; Jianhong Lu[1,2]; Shuyuan Guo[1,2,3]; Ningning Liang[1,2]; Jing Ge[1,2]; Mingjiang Zhu[1]; Yongzhen Tao[1]; Yun-Cheng Wu[4], and Huiyong Yin[1-3,5*]

[1] CAS Key Laboratory of Nutrition, Metabolism and Food Safety, Shanghai Institute of Nutrition and Health, Shanghai Institutes for Biological Sciences (SIBS), Chinese Academy of Sciences (CAS), Shanghai 200031, China

[2] University of Chinese Academy of Sciences, CAS, Beijing 100049, China

[3] School of Life Science and Technology, ShanghaiTech University, Shanghai 200031, China

[4] Department of Neurology, Shanghai General Hospital, Shanghai Jiao Tong University School of Medicine, Shanghai, China

[5] Key Laboratory of Food Safety Risk Assessment, Ministry of Health, Beijing, 100000, China

The authors have declared that no conflict of interest exists.

Address for Correspondence: Huiyong Yin, PhD**,** Room 1826, New Life Science Bldg., 320 Yueyang Rd., Shanghai Institute of Nutrition and Health, Shanghai Institutes for Biological Sciences, Chinese Academy of Sciences, Shanghai, China, 200031.

E-mail: hyyin@sibs.ac.cn; Tel: (86)-21-54920942

Abstract

Aldehyde dehydrogenase 2 (ALDH2) is a mitochondrial enzyme detoxifying acetaldehyde and endogenous lipid aldehydes; previous studies suggest a protective role of ALDH2 against cardiovascular disease (CVD). Around 40% of East Asians carrying a single nucleotide polymorphism (SNP) ALDH2 rs671 have increased incidences of CVD. However, the role of ALDH2 in CVD beyond alcohol consumption remains poorly defined. Here we report that *ALDH2/LDLR* DKO mice have decreased atherosclerosis compared to *LDLR* KO mice, whereas *ALDH2/APOE* DKO have increased atherosclerosis, suggesting an unexpected interaction of ALDH2 with LDLR. Further studies demonstrate that in the absence of LDLR, AMPK phosphorylates ALDH2 at threonine 356 and enables its nuclear translocation. Nuclear ALDH2 interacts with HDAC3 and represses transcription of a lysosomal proton pump protein ATP6V0E2, critical for maintaining lysosomal function, autophagy and degradation of oxLDL. Interestingly, an interaction of cytosolic LDLR C-terminus with AMPK blocks ALDH2 phosphorylation and subsequent nuclear translocation, whereas ALDH2 rs671 mutant in human macrophages attenuates this interaction, which releases ALDH2 to nucleus to suppress *ATP6V0E2* expression, resulting in increased foam cells due to impaired lysosomal function. Our studies reveal a novel role of ALDH2 and LDLR in atherosclerosis and provide a molecular mechanism by which ALDH2 rs671 SNP increases CVD.

Introduction

Atherosclerosis is the major cause for cardiovascular disease (CVD) and macrophages play a central role in progression of atherosclerosis (1, 2). In the early stage of atherosclerosis, macrophages take up the oxidized low-density lipid protein (ox-LDL) through scavenger receptors and degrade it in lysosomes. The importance of lysosomal functions in macrophage foam cell formation has been increasingly recognized and recent studies identified that autophagy and lysosome function were critically involved in cholesterol metabolism and the over-expression of cholesteryl ester hydrolase in macrophage significantly reduces atherosclerosis (3, 4). Dysfunctional lysosomes may lead to the accumulation of lipids and foam cell formation, an early hallmark of atherosclerosis (5, 6). Furthermore, a recent study explored autophagy-lysosomal biogenesis as a potential therapeutic strategy for atherosclerosis (5, 7).

LDL receptor (LDLR) is an important factor for maintaining cholesterol homeostasis. LDLR is a cell-surface receptor that removes the cholesterol-rich LDL from plasma and maintains the cholesterol level in the blood circulation (8). The protein is encoded by *LDLR* gene on chromosome 19, synthesized in ER, matured in Golgi, and finally transferred to the cytoplasm membrane. LDLR has close relationship with the development of atherosclerosis. Human subjects with at least one LDLR abnormal allele manifest high LDL-C level in their blood, termed familial hypercholesterolemia (FH), with significantly increased risk of coronary artery disease (CAD) due to the inefficient removal of LDL from the circulation (9, 10). Two mouse models, LDLR–deficient (*LDLR* KO) (11) and apoprotein E–deficient (*APOE* KO), have been extensively used for studying atherosclerosis since 1990s (12). Moreover, proprotein convertase subtilisin/kexin type 9 (PCSK9) binds to LDLR and accelerates the degradation of LDLR. PCSK9 has been explored as an attractive drug target for treating hypercholesterolemia and atherosclerosis (13, 14).

Acetaldehyde dehydrogenase 2 (ALDH2) is the mitochondrial isoform of aldehyde dehydrogenases which plays a key role in the metabolism of ethanol-derived acetaldehyde

and other toxic lipid aldehydes generated from lipid peroxidation under oxidant stress (15). Some previous evidence suggests that ALDH2 protects cardiovascular diseases (CVD) through detoxification of endogenous lipid aldehydes, such as 4-hydroxy-2-nonenal (4-HNE) (16) and inhibiting inflammation in endothelial cells (ECs) (17). Moreover, 30-50% of East Asians possess an ALDH2 rs671 mutant which is responsible for alcohol-flush reaction due to the poor metabolism of ethanol resulted from significant loss of ALDH2 enzymatic activity in heterozygotes and homozygotes carrying ALDH2 SNP rs671 (18, 19). Epidemiological studies have shown that humans carrying ALDH2 rs671 SNP are positively correlated with an increased risk of CVD and the toxic effects of alcohol-derived acetaldehydes have been postulated to be primarily responsible for this cardiovascular liability (20). Paradoxically, however, humans with ALDH2 SNP tend to consume much less alcohol compared to the non-carriers and the underlying mechanisms related to CVD beyond alcohol consumption remain largely unexplored.

In this study, we discovered a novel pro-atherogenic effects of ALDH2, independent of its enzymatic activity. We made a serendipitous observation in that *ALDH2/LDLR* double knockout (DKO) mice had significantly decreased atherosclerotic plaques compared to *LDLR* KO mice, which is opposite to *ALDH2/APOE* DKO mice. Macrophages are the major cell types responsible for this phenotype. We further demonstrate that macrophages ALDH2 promotes atherosclerosis by causing impaired lysosomal function and autophagy through interaction with AMPK, which leads to increased lipid deposition and foam cell formation due to impaired cholesterol hydrolysis in lysosome; LDLR with its cytosolic C-terminus blocks the interaction of ALDH2 and AMPK. Furthermore, even in the presence of LDLR, human ALDH2 rs671 mutant attenuates the interaction of LDLR and ALDH2 and increases the interaction of AMPK and ALDH2, which recapitulates the phenotype in *LDLR* KO mice with increased atherosclerosis. Our study has identified a novel molecular mechanism by which interaction of ALDH2 and LDLR regulates macrophage foam cell formation. This mechanism may apply to humans with ALDH2 SNP rs671 who have increased incidence of CVD independent of

alcohol consumption. Furthermore, our study warrants future investigation into whether AMPK activation by the widely-used antidiabetic medication, Metformin, potentially increases the risk of atherosclerosis in humans with ALDH2 rs671 SNP.

Results

ALDH2/LDLR DKO attenuates atherosclerotic plaque formation compared to LDLR KO mice, whereas ALDH2/APOE DKO shows increased plaque areas compared to APOE KO mice

To investigate the role of ALDH2 in atherosclerosis, we crossed *ALDH2* KO mice onto *LDLR* KO background mice to generate *ALDH2/LDLR* DKO mice and then fed Western Diet (WD) for 12 weeks and 26 weeks, respectively. Surprisingly, compared with *LDLR* KO, although the body weight (BW), ratios of heart weight to body weight, levels of total glycerides (TG) and total cholesterol (TC) were not significantly changed (Figure S1A-S1D, n=9-10), *en face* areas of atherosclerotic lesions in aorta were significantly decreased in male *ALDH2/LDLR* DKO mice at two different time points (Figure 1A, 4.13% ± 0.52% vs 2.06% ± 0.30%, $p<0.01$, n=8 at 12 weeks, Figure 1B; 23.12% ± 0.93% vs 15.31% ± 1.13%, $p<0.001$, n=9-10 at 26 weeks, Figure 1C). To validate the phenotype, we replicated the 26-week time point and found similar trend (*ALDH2/LDLR* DKO vs *LDLR* KO: 20.40% ± 1.41% vs 15.16% ± 0.78%, $p<0.01$, n=15) (supplemental Figure S1E). And consistent with en face results, H&E staining for aortic root lesions showed that *LDLR* KO mice had more aortic root lesions than *ALDH2/LDLR* KO mice (male, 12w and 26w, Supplemental Figure S1F). Same trends were also observed for female mice (supplemental Figure S1G, 3.81% ± 0.37% vs 2.06% ± 0.26%, $p<0.01$, n=9 at 12 weeks, supplemental Figure S1H; 14.59% ± 1.01% vs 9.923% ± 0.93%, $p<0.01$, n=8, at 26 weeks, supplemental Figure S1I). These observations were contrary to those in *ALDH2/APOE* DKO mice in which *ALDH2/APOE* KO had significantly increased atherosclerotic area compared to *APOE* KO (4.24% ± 0.25% vs 6.98% ± 0.92%, $p<0.01$, n=7-9 at 12 weeks, Figure 1D), consistent with a previous study in which ALDH2 knockdown by *ALDH2*-RNAi lentivirus promoted atherosclerosis in *APOE* KO mice with increased plaque

area, more macrophage infiltration, less collagen and smooth muscle cells (supplemental Figure S2A) (17).

We next examined the cell types responsible for the decreased plaque formation in *ALDH2/LDLR* DKO mice by immunohistochemical (IHC) staining of collagen (stained by Masson staining), α-smooth muscle cells (SMCs) and macrophages (CD68) in mouse aorta. In *ALDH2/LDLR* DKO mice, we found that macrophages were significantly decreased after 12 weeks ($P<0.05$, Figure 1E) and 26 weeks of WD feeding ($P<0.05$, supplemental Figure S2B), respectively, whereas the SMC were slightly decreased only at 26 weeks. Then, to further examine the roles of macrophages in decreasing atherosclerosis with *ALDH2* KO in *LDLR* KO background, we transplanted the bone marrow of *ALDH2/LDLR* DKO and *LDLR* KO mice to *LDLR* KO and *ALDH2/LDLR* DKO mice, respectively, and fed WD for 12 weeks after 8 weeks recovery. Analysis of *en face* atherosclerotic lesions showed that transplanting *ALDH2/LDLR* DKO bone marrow to *LDLR* KO decreased the formation of atherosclerotic plaque compared to transplanting bone marrow of *LDLR* KO to *LDLR* KO mice (Figure 1F, 1.9% ± 0.27% vs 0.97% ± 0.20%, $P<0.01$, n=9). Consistently, transplanting bone marrow of *ALDH2/LDLR* DKO to *ALDH2/LDLR* DKO mice had decreased atherosclerotic plaques compared to *LDLR* KO to *ALDH2/LDLR* DKO (Figure 1F, 2.317% ± 0.43% vs 0.49% ± 0.13%, $P<0.01$, n=9). All these data show that macrophages are primarily responsible for the decreased atherosclerosis in *ALDH2/LDLR* DKO mice compared to *LDLR* KO mice.

Taken together, *ALDH2* KO on a *LDLR* KO background significantly decreased the atherosclerotic plaque formation, contrary to the phenotypes observed in *ALDH2* KO on *APOE* KO background, suggesting an unexpected mechanism involving an interaction of ALDH2 with LDLR in macrophages.

ALDH2 regulates macrophage foam cell formation in an LDLR-dependent manner through modulation of lysosomal function and cholesterol ester (CE) hydrolysis

It is well-established that macrophage foam cells are formed from excessive accumulation of oxidized LDL (oxLDL). We next examined the macrophage phagocytotic capability with different genetic background and found that comparing to *ALDH2/LDLR* DKO, *LDLR* KO led to the increased levels of oxLDL and CE, a hallmark of macrophage foam cells (Figure 2A to 2B), whereas *ALDH2* KO has no effect on oxLDL and CE in the present of LDLR (supplemental Figure S3A to S3B), consistent with the hypothesis that ALDH2 affects foam cell formation by interaction with LDLR. These in vitro observations were consistent with the decreased plaque formation in *ALDH2/LDLR* DKO compared to LKO mice.

Macrophages play an important role in cholesterol homeostasis through balancing oxLDL uptake, degradation (hydrolysis in lysosome), and efflux. Dysregulation of any of these processes may eventually lead to foam cell formation. We next investigated whether the oxLDL binding was regulated by ALDH2 and found that the binding of oxLDL did not change significantly in *LDLR* KO and *ALDH2/LDLR* DKO macrophages or WT and *ALDH2* KO macrophages (Figure 2C and supplemental Figure S3C), consistent with the similar expression levels of the three major scavenger receptors responsible for ox-LDL uptake (LOX1, SRA, and CD36) (Figure 2D and supplemental Figure S3D). These results suggest that the interaction of ALDH2 with LDLR does not affect binding of ox-LDL in macrophages. Then, we measured the hydrolysis of CE and the expression of lysosome function markers (LAMP1) in macrophages from *LDLR* KO and *ALDH2/LDLR* DKO mice after treatment with oxLDL (Figure 2E to 2F). Interestingly, CE hydrolysis and LAMP1 expression were significantly decreased in *LDLR* KO macrophages comparing to *ALDH2/LDLR* DKO (Figure 2E to 2F) but not changed in WT and *ALDH2* KO macrophages (supplemental Figure S3E to S3F), suggesting that in the absence of LDLR, ALDH2 impairs lysosomal function and CE hydrolysis but this effect is lost when LDLR is present. Then, we measured cholesterol efflux in different genetic macrophages and found that cholesterol efflux was also increased in oxLDL-loaded *ALDH2/LDLR* DKO macrophages compared to *LDLR* KO (Figure 2G) but not significantly changed in WT and *ALDH2* KO macrophages (supplemental Figure S3G).

Interestingly, however, the expressions of the transporter responsible for cholesterol efflux, ABCA1, and enzyme for cholesteryl ester formation, ACAT1, were not significantly changed (Figure 2H, supplemental Figure S3H and S4), suggesting that the increased efflux was most likely due to the increased lysosomal hydrolysis of CE instead of subsequent re-esterification of cholesterol and efflux.

Collectively, these data demonstrate that the interaction of ALDH2 and LDLR affects the foam cell formation primarily through modulating macrophage lysosomal function (*vide infra*) without changing the binding, re-esterification of cholesterol, nor expressions of transporter ABCA1 for cholesterol efflux.

Decreased macrophage foam cell formation in ALDH2/LDLR DKO comparing to LDLR KO is due to the increased lysosomal function and autophagy

Immerging evidence demonstrates that endocytosis and autophagy are important for oxLDL metabolism in macrophages. We next examined how these two functions were involved in the decreased foam cells formation in *ALDH2/LDLR* DKO macrophages due to the interaction of LDLR and ALDH2. We found that the expression of RAB7 was significantly elevated (Figure 3A) while the protein levels of LC3 II and P62 were significantly decreased in *ALDH2/LDLR* DKO macrophages compared to those from *LDLR* KO mice (Figure 3B), suggesting that *ALDH2/LDLR* DKO rescued the impaired autophagy by increasing lysosomal function which leads to an increased endocytosis (increased expression of RAB7, Figure 3A and supplemental Figure S5A) and autophagic flux (decreased expression of P62, Figure 3B). Consistently, fluorescent confocal microscopy indicated that the number of autolysosome (RFP, indicator of an acidic environment, which is critical for maintaining normal lysosome function) was increased in *ALDH2/LDLR* DKO macrophages and this increase was completely diminished by treatments with autophagic inhibitors chloroquine (CQ) or Bafilomycin A1 (Baf-A1) to neutralize lysosomal pH (Figure 3C). Interestingly, Leupeptin A (Leu), an inhibitor of autophagy without affecting lysosomal pH, did not affect the increase of autolysosome

numbers in macrophages of *ALDH2/LDLR* DKO compared to *LDLR* KO, suggesting that ALDH2 regulates autophagy through modulation of lysosomal function. Moreover, Baf-A1 also diminished the increased uptake of ox-LDL in *LDLR* KO macrophages to the same level as those in *ALDH2/LDLR* DKO macrophages (Figure 3D). These observations agreed with the fact that comparing to *ALDH2/LDLR* DKO macrophages, accumulation of CE caused by the decreased CE hydrolysis in *LDLR* KO macrophages and Baf-A1 treatment completely eliminated these differences (Figure 3E to 3F). Interestingly, autophagic flux is inhibited in *ALDH2* KO macrophages comparing to WT macrophages without a significant change of endocytosis, oxLDL uptake, CE content and hydrolysis (supplemental Figure S5C to S5F), consistent with the hypothesis that ALDH2 interacts with LDLR and regulates autophagy. Taken together, these results demonstrate that impaired lysosomal function is responsible for foam cell formation in *LDLR* KO macrophages and this effect is eliminated in *ALDH2/LDLR* DKO mice, suggesting that ALDH2 interacts LDLR to cause lysosomal dysfunction and foam cell formation in macrophages through some unknown mechanisms.

LDLR modulates nuclear translocation of ALDH2 through physical binding to ALDH2 and ALDH2 rs671 mutant decreases this interaction

To explore the underlying mechanism by which ALDH2 regulates macrophage foam cell formation through interaction with LDLR, we first examined ALDH2 enzymatic activity in macrophages from mice with different genetic background. We found that knocking out ALDH2 alone or in the absence of LDLR (*ALDH2/LDLR* DKO) almost completely destroyed the ALDH2 activity (Figure S5G), whereas ALDH2 activity was not changed in WT and *LDLR* KO macrophages. However, foam cell formation was significantly attenuated in *ALDH2/LDLR* DKO compared to *LDLR* KO, suggesting that LDLR and ALDH2 interactions on foam cell formation are independent of its enzymatic function. These observations prompted us to hypothesize that ALDH2 may exert a non-enzymatic function presumably by translocation to the nucleus to regulate genes important for lysosomal function and autophagy and LDLR

blocks this nuclear translocation by physically binding to ALDH2. To support this hypothesis, we first performed Co-immunoprecipitation (Co-IP) experiments with Myc-tagged LDLR and Flag tagged ALDH2 in 293T cells. As shown in supplemental Figure S6A, LDLR and ALDH2 appeared to physically bind together. Similar results were observed in primary macrophage cells (Figure 4A). Importantly, ALDH2 rs671 SNP mutant attenuates the binding with LDLR (Figure 4B). To investigate how LDLR interacts with ALDH2, we truncated C terminus of LDLR and found that this truncation caused completely loss of binding to ALDH2 (Figure 4C), whereas a mutant (N812A) at C-terminus of LDLR significantly attenuated the binding of ALDH2 to LDLR (Supplemental Figure S6B), suggesting that C terminus in the cytosolic region of LDLR is the critical region of binding to ALDH2. Next, we carried out Immunofluorescence (IF) experiments and found out that ALDH2 translocated to nucleus in the absence of LDLR, whereas LDLR expression in WT inhibited this translocation (Supplemental Figure S6C). Similarly, a gene dose effect was observed for LDLR to inhibit the nuclear translocation of ALDH2: heterozygous *LDLR*$^{+/-}$ has intermediate effect compared to *LDLR* KO. In addition, upregulation of LDLR by cholesterol depletion has similar effect on inhibition of ALDH2 nuclear translocation as that in WT macrophages (Figure 4D and 4E). Interestingly, ALDH2 rs671 mutant promoted ALDH2 translocation even in the presence of LDLR (Supplemental Figure S6D and S6E). Together, all these data strongly support the hypothesis that LDLR regulates the nuclear translocation of ALDH2 through physical binding to ALDH2, whereas ALDH2 rs671 mutant decreases this interaction.

AMPK promotes ALDH2 translocation by phosphorylating ALDH2 in macrophages in the absence of LDLR or ALDH2 rs671 mutant

Previous studies suggested that ALDH2 was a substrate for AMPK (21) and we hypothesized that phosphorylated ALDH2 by AMPK played an important role in regulating ALDH2 nuclear translocation. To determine whether ALDH2 was phosphorylated by AMPK in *LDLR* KO macrophages, we performed high resolution mass spectrometry-based

phosphoproteomics to identify the potential phosphorylation sites of ALDH2 in *LDLR* KO macrophages. In *LDLR* KO macrophages, we identified two phosphorylation sites: threonine 356 (T356, Supplemental Figure S7A) and tyrosine 148 (Y148, Supplemental Figure S7B). Furthermore, in *LDLR* KO macrophages treated with an AMPK agonist, AICAR, we further confirmed the phosphorylation at T356 (Supplemental Figure S7A), demonstrating that AMPK phosphorylates ALDH2 at T356 in *LDLR* KO macrophages. To provide further evidence that AMPK could phosphorylate ALDH2, we performed Co-IP experiments and demonstrated that ALDH2 indeed interacted with AMPK in 293T cells (Supplemental Figure S8A) and *LDLR* KO BMDM (Figure 4F). Moreover, ALDH2 rs671 mutant increased the binding of ALDH2 and AMPK but decreased the binding of ALDH2 and LDLR (Figure 4G, Supplemental Figure S8B). Interestingly, we also observed a gene dose effect of LDLR on inhibition of ALDH2 phosphorylation in *LDLR* $^{-/-}$ and *LDLR* $^{+/-}$ macrophages: increased expression of LDLR from -/- to +/- led to a decreased ALDH2 phosphorylation and upregulation of LDLR by cholesterol depletion further inhibited ALDH2 phosphorylation (Supplemental Figure S8C). Next, to investigate whether AMPK enabled translocation of ALDH2 to the nucleus, we performed nuclear fractionation experiments and found that more ALDH2 translocated into nucleus in *LDLR* KO BMDMs with AICAR treatment (Figure 5A). Moreover, ALDH2 rs671 mutant promoted ALDH2 translocation, which is consistent with the increased binding with AMPK (Figure 5B). To further confirm that AMPK promoted ALDH2 translocation, we performed a time course study with AMPK activation and demonstrated that ALDH2 initially resided in mitochondria and AMPK activation by AICAR enabled the translocation from mitochondria to nucleus as indicated by the increased green fluorescence at 60 and 90 mins (Supplemental Figure S8D). Furthermore, a widely used anti-diabetic agent and known AMPK activator, Metformin, also increased ALDH2 translocation, whereas inhibition of AMPK by Compound C (CC) blocked the nuclear translocation of ALDH2 in LKO macrophages (Figure 5C-D). Moreover, we transfected retrovirus with LDLR and GFP (GFP-TRV-LDLR) in *LDLR* KO BMDMs and observed that LDLR blocked the translocation of ALDH2 to nucleus in LKO

BMDMs (Figure 5E). Furthermore, the nuclear translocation of ALDH2 can be blocked by expression of LDLR in *LDLR* KO macrophages even in the presence of AICAR (Figure 5E-F). Next, we found that Metformin dose-dependently increased the phosphorylation of ALDH2 in *LDLR* KO macrophages (Figure 5G) but not in WT macrophages (Supplemental Figure S8E). Taken together, these results unambiguously demonstrated that AMPK phosphorylated ALDH2 and enabled its nuclear translocation in the absence of LDLR or in ALDH2 rs671 mutant.

LDLR inhibits the binding of ALDH2 with AMPK and loss of LDLR leads to the increased activation of AMPK in macrophages

We next investigated how ALDH2, LDLR, and AMPK interact. Firstly, we found that LDLR KO increased the phosphorylation of AMPK (Figure 6A). Intriguingly, however, we did not observe significant changes for the mRNA levels of the upstream genes of AMPK: *Lkb1*, *Camkk2*, *Mo25, Strad*, and *Tak1* (Supplemental Figure S9A). Furthermore, there is no difference for the levels of AMP, ADP, ATP, and AMP/ATP, with or without oxLDL in *LDLR* KO and WT macrophages (Figure 6B, Supplemental Figure S9B-S9D). These results suggest that AMPK activation by *LDLR* KO is not likely through conventional pathways instead LDLR might physically interfere the phosphorylation of AMPK through interacting with AMPK and thereby inhibit the binding of ALDH2 to AMPK. To support our hypothesis, we performed Co-IP experiments in WT and *LDLR* KO BMDMs and found that LDLR blocked the interaction of ALDH2 and AMPK (Figure 6C). In 293T cell, we found that overexpression of ALDH2 or AMPK, both proteins bound to LDLR whereas LDLR only interacted with ALDH2 and AMPK when LDLR was overexpressed (Figure 6D-6F). These results demonstrate that ALDH2 and AMPK preferentially interact with LDLR when LDLR presents, suggesting that physical interaction of LDLR and AMPK presumably blocks the phosphorylation sites of AMPK. Consistently, AMPK is activated (increased levels of P-AMPK) in the absence of LDLR without affecting the upstream genes of AMPK (Figure 6A).

AMPK plays an important role in regulating endocytosis and autophagy for LDLR-regulated ox-LDL metabolism in macrophages

To confirm the role of AMPK in regulating foam cell formation through modulating lysosomal function and autophagy, we treated LKO and WT macrophages with CC and Metformin, respectively. As expected, LAMP1 expression was increased by AMPK inhibition with CC treatment but decreased by AMPK activation with Metformin (Figure 6G, Supplemental Figure S10A) in ox-LDL loaded *LDLR* KO macrophages. Furthermore, to examine how AMPK regulates endocytosis and autophagy, we further showed that in *LDLR* KO BMDMs, AMPK activation by Metformin decreased endocytosis (decreased RAB7 expression) and autophagy (increased P62 and LC3 II expression), whereas AMPK inhibition by CC led to increased endocytosis (increased RAB7 expression) and autophagy (decreased P62 and LC3 II expression) (Figure 6H-6I). Consistently, in WT BMDMs, AMPK activation by Metformin increased autophagy (decreased P62), whereas AMPK inhibition by CC led to a decreased autophagy (increased P62) without affecting endocytosis (Supplemental Figure S10B-C). Notably, AMPK activation or inhibition only affects the protein levels of P62 without change its transcription (Supplemental Figure S11). Next, we found that AMPK activation by Metformin promoted foam cell formation by decreasing CE hydrolysis while AMPK inhibition by CC treatment significantly attenuated foam cell formation by increasing CE hydrolysis in ox-LDL loaded *LDLR* KO macrophages (Figure 6J to 6K). Together, these results demonstrate that AMPK mediates ox-LDL metabolism, autophagy and foam cell formation through the interactions with ALDH2 and LDLR.

Nuclear translocated ALDH2 regulates lysosomal function through downregulation of the transcription of Atp6v0e2 in LDLR KO or ALDH2 rs671 mutant

To investigate the functional consequences after ALDH2 enters nucleus, we performed transcriptomic RNA-Seq analysis to mapping the genes that were regulated by ALDH2 by

using *ALDH2/LDLR* DKO and *LDLR* KO macrophages (Supplemental Figure S12-S15). We found that a lysosomal function-related gene *Atp6v0e2*, coding H^+-ATPase, was ranked at the 3rd most upregulated genes (Supplemental table 1). Due to the importance of lysosomal function and cholesterol efflux in macrophage metabolism of oxidized LDL, *ATP6V0E2* mRNA levels were further validated by quantitative PCR (Supplemental Figure S16). The expressions of ATP6V0E2 were significantly regulated by LDLR: there was no significant difference between the RNA levels of *Atp6v0e2* in WT and *ALDH2* KO whereas *Atp6v0e2* was significantly downregulated in *LDLR* KO, consistent with the increased uptake of ox-LDL in *LDLR* KO and decreased expression of lysosomal biogenesis protein LAMP1 (Figure 2A-B, F). Interestingly, even though the mRNA levels of *Atp6v0e2* in *ALDH2/LDLR* DKO was higher than those from WT, *ALDH2* KO and *LDLR* KO (about 20-folds for *LDLR* KO), ATP6V0E2 protein level in LDLR KO macrophages was half of those in WT, *ALDH2* KO and *ALDH2/LDLR* DKO macrophages (Figure 7A). Moreover, we examined the protein expression of ATP6V0E2 in the macrophages of aorta from *LDLR* KO and *ALDH2/LDLR* DKO mice fed WD for 12 and 26 weeks, respectively, by Immunofluorescence (green, CD68, marker for macrophages; red, ATP6V0E2). As shown in Figure 7B, ATP6V0E2 expression was significantly increased in aorta from *ALDH2/LDLR* DKO mice compared with *LDLR* KO, consistent with the hypothesis that expression of ATP6V0E2 is important for regulating foam cell formation. Moreover, co-overexpressed AMPK and ALDH2 in 293T cells significantly decreased ATP6V0E2 expression (Figure 7C). Over-expressed AMPK and a mutant ALDH2 T356A site did not change ATP6V0E2 expression while WT and mutant ALDH2 Y148A decreased ATP6V0E2 expression (Figure 7D). Similar results were obtained in the treatment with Metformin (Supplemental Figure S17). These results demonstrated that T356 in ALDH2 rather than Y148 was responsible for regulating ATP6V0E2 expression by AMPK. Furthermore. LDLR dose-dependently decreased ALDH2 phosphorylation and increased ATP6V0E2 expression in 293T cells (Supplemental Figure S18A). Moreover, our previous data demonstrated that LDLR C-terminus was involved in the interaction of LDLR and ALDH2 (Figure 4C, Supplemental

Figure S6B). To further investigate if this interaction regulates ATP6V0E2 expression, we inhibited endocytotic pathway by knocking down the expression of clathrin heavy chain (CHC) and observed that inhibiting LDLR entered cytoplasm decreased ATP6V0E2 expression through downregulation of RAB5 and RAB7 (Supplemental Figure S18B). Next, to find how ALDH2 regulates ATP6V0E2, we tested the interactions of ALDH2 and HDAC family by Co-IP in macrophages and found that ALDH2 had stronger interaction with HDAC3 in *LDLR* KO BMDMs (Figure 7E). We next performed Chromatin Immunoprecipitation (ChIP) assay to investigate whether ALDH2 bound to HDAC3 and regulated the transcription of *ATP6V0E2*. We designed the primers on the promoter region stretched over a transcription start site (TSS) of *ATP6V0E2* and found that ALDH2 regulated the transcription of *ATP6V0E2* in *LDLR* KO BMDMs and AMPK activation by AICAR enhanced this effect (Figure 7F). Next, we constructed *ATP6V0E2* promoter-luciferase plasmid and studied luciferase activity to test whether ALDH2 could regulate the transcriptional activity of *ATP6V0E2*. As shown in Figure 7G, ALDH2 indeed increased the luciferase activity of *ATP6V0E2*, which was further enhanced by treating with AICAR in 293T cells. To further examine the role of HDAC3 in ALDH2 regulation of *ATP6V0E2*, we performed ChIP experiment to measure the binding of HDAC3 to *ATP6V0E2* promoter in *LDLR* KO and *ALDH2/LDLR* DKO BMDMs treated with Metformin. In Supplemental Figure S19A, consistent with previous data, HDAC3 only bound to *ATP6V0E2* promoter in the presence of ALDH2. Moreover, we also used an HDAC3-specific inhibitor RGF966 to treat the macrophages from *LDLR* KO and WT mice. Inhibition of HDAC3 led to the increased levels of H3K27ac in both WT and *LDLR* KO macrophage while the decreased expression of ATP6V0E2 in *LDLR* KO macrophages was rescued to the same levels as WT (Supplemental Figure S19B). Furthermore, ALDH2 rs671 mutant also increased the regulation of *ATP6V0E2* transcriptional activity (Figure 7H) and resulted in decreased the protein expression of ATP6V0E2 (Figure 7I).

Taken together, our data demonstrate that in the macrophages of *LDLR* KO or *ALDH2* rs671 mutant, AMPK phosphorylates ALDH2 at T356, which enables its nuclear translocation.

Once in the nucleus, ALDH2 binds to HDAC3 and suppresses the transcription and protein expression of ATP6V0E2.

Human macrophages from subjects carrying ALDH2 rs671 SNP have increased foam cell formation caused by the downregulation of ATP6V0E2 and autophagy due to increased nuclear translocation of ALDH2

To investigate the clinical relevance of ALDH2-regulated macrophage formation, we recruited human subjects carrying *ALDH2* rs671 SNP (heterozygous *ALDH2*2/2*1*, n=10) and control (*ALDH2*1*, n=16) to isolate peripheral blood monocytes (PBMC). After differentiation into macrophages, we treated the cells with oxLDL and observed a significantly decreased *ATP6V0E2* mRNA levels in macrophages from *ALDH2*2/2*1* compared to *ALDH2*1* (Figure 8A). Furthermore, ATP6V0E2 protein levels were significantly decreased while the P62 levels were increased in *ALDH2*2/2*1* compared to *ALDH2*1* (Figure 8B), suggesting an impaired autophagy due to the downregulation of ATP6V0E2. Consistently, the cholesterol ester hydrolysis was significantly attenuated in *ALDH2*2/2*1* macrophages (Figure 8C). Furthermore, confocal studies clearly indicated that more ALDH2 translocated into nucleus in *ALDH2*2/2*1* macrophages and this effect was augmented upon AMPK activation by Metformin treatment (Figure 8D). These in vitro studies provide strong evidence that human *ALDH2* SNP rs671 potentially promotes atherosclerosis through modulation of macrophage foam cell formation, which represents a novel molecular mechanism by which *ALDH2* rs671 polymorphism increases the risk of CVD. Interestingly, our study suggests that Metformin may increase the risk of atherosclerosis in humans with *ALDH2* rs671 SNP, which warrants future investigation.

Discussion

CVD remains the leading cause of deaths worldwide and atherosclerosis is the major factor underlying CVD (22). A body of epidemiological evidence has linked the *ALDH2* SNP

rs671 (E487K) to an increased risk of CVD in around 40% of East Asians carrying this SNP but the underlying molecular mechanisms remain poorly defined (23). ALDH2 primarily resides in mitochondria and exerts a detoxification function of ethanol-derived acetaldehyde and other endogenous lipid aldehydes, such as 4-HNE. Previous studies supported a protective role of ALDH2 in CVD based on the detoxification function and the toxic effects of acetaldehyde has been postulated to be responsible for this cardiovascular effect. Paradoxically, the carriers of ALDH2 SNP rs671 tend to consume less alcohol comparing to the non-carriers; thus the underlying mechanism for the association of *ALDH2* SNP and CVD independent of alcohol remains to be investigated. Our study has identified a novel molecular mechanism by which *ALDH2* SNP rs671 increased atherosclerosis through AMPK-phosphorylated ALDH2 translocating into nuclear and then repressing the gene expression of *ATP6V0E2* which is responsible for maintaining normal lysosomal function, autophagy and ox-LDL degradation (Figure 9).

It is well-established that dysregulation of cholesterol metabolism leads to atherosclerosis. In macrophages, after binding to LDLR, LDL is transferred to lysosome through endosome, whereas oxidized LDL is primarily taken up by the scavenger receptors through endocytosis. CE in LDL and oxLDL can be hydrolyzed in lysosome; thus, a normal lysosomal function and autophagy is critical for CE hydrolysis and cholesterol efflux. Conversely, impaired lysosomal function and autophagy may lead to the accumulation of excessive CEs to form foam cells, an early hallmark of atherosclerosis. For the first time, our studies identified that ALDH2 can be phosphorylated by AMPK at T356 and translocate into nucleus, interact with HDAC3, and repress the expression of ATP6V0E2, a lysosomal proton pump protein that plays a critical role in the fusion of lysosome with endosome or autophagosome (Figure 9). Under normal circumstances, this process is blocked by LDLR to ensure normal endocytosis and autophagy to avoid excessive lipid accumulation to form foam cells. However, importantly, when LDLR is knocked out (in the case of LDLR KO) or interaction between LDLR and mutant ALDH2 (with human SNP rs671) is weakened, ALDH2 is

phosphorylated by AMPK and translocated into nucleus, which eventually leads to a dysfunctional lysosome and impaired CE hydrolysis. We provide evidence that LDLR most likely interacts with ALDH2 and AMPK with its cytosolic C terminus to block the nuclear translocation of ALDH2. This serendipitous discovery was made from an unexpected observation of a phenotypic discrepancy in *ALDH2* KO in LDLR and APOE background. More importantly, we have uncovered a novel mechanism by which *ALDH2* SNP rs671 increases atherosclerosis and a novel role of AMPK in macrophages for increasing this potentially detrimental effect of ALDH2 in the context of atherosclerosis.

Previous studies have provided evidence that ALDH2 plays an important role in cardiac protection against myocardial infarction primarily based on the fact that ALDH2 is an important enzyme responsible for eliminating toxic aldehydes. Selective activation of ALDH2 improved the heart failure outcome by reducing toxic aldehyde overload and restoring mitochondrial function (24). Moreover, ALDH2 appears to protect against MI-related cardiac fibrosis through modulation of the Wnt/β-catenin signaling pathway (25). Comparing to the cardiac protection, the roles of ALDH2 in atherosclerosis remain poorly defined. A recent epidemiological study in East Asian populations using alcohol flushing status as an instrumental variable demonstrated that increased alcohol consumption was positively associated with an increased risk of subclinical coronary atherosclerosis, suggesting that ALDH2 might be involved in the pathogenesis of atherosclerosis (26). A previous study using *APOE* KO mice transfected with ALDH2-overexpression or ALDH2-RNAi lentivirus found that ALDH2 had a protective role in atherosclerosis through attenuating the inflammation in endothelial cells (17). Similarly, we observed increased atherosclerotic plaques in *ALDH2/APOE* DKO mice. However, *ALDH2/ LDLR* DKO had much less atherosclerotic lesions than the *LDLR* KO mice. This unexpected observation led us to discover a non-enzymatic role of ALDH2, which promotes foam cell formation by translocating to the nucleus after phosphorylated by AMPK to repress ATP6V0E2 expression, a critical protein for lysosomal function and autophagy. The phenotypic discrepancy in DKO mice of ALDH2 with APOE and LDLR is most likely due to the different

roles of inflammation and LDLR-regulated ALDH2 nuclear translocation. In *APOE* KO mice, the mechanism identified in current study does not operate due to the presence of LDLR which blocks the nuclear translocation of ALDH2, whereas in *APOE/ALDH2* DKO mice, increased atherosclerotic plaque formation compared to *APOE* KO mice is primarily due to the elevated inflammation in endothelial cells (17). On the other hand, *ALDH2/LDLR* DKO had decreased atherosclerosis compared to *LDLR* KO primarily through attenuated foam cell formation in macrophages in addition to attenuated inflammation. As one of the most important types of immune cells in atherogenesis, macrophages are critical for inflammatory responses and the formation of foam cell (27, 28). Macrophages tend to polarize to different phenotypes upon exposure to oxidized lipids (28). Consistent with the decreased atherosclerotic lesions in *ALDH2/LDLR* DKO mice, the DKO macrophages exhibited an anti-inflammatory M2 phenotype, whereas the markers for M1 phenotype was significant decreased despite the fact that other inflammation markers were increased in plasma and endothelial cells (Supplemental Figure S20). These data appear to suggest that the mechanisms identified in this study play a predominant role in the atherosclerosis in the context of foam cell formation.

The most exciting discovery of our current study is that AMPK-phosphorylated ALDH2 translocates to nucleus and represses *ATP6V0E2*, a protein critical for lysosomal function, endocytosis and autophagy. ATP6V0E2 belongs to the H^+-ATPase family that is important for the lysosomal proton pump to maintain the proper function of the lysosomes (29). Many proteins belong to this family (V-ATPase) other than ATP6V0E2 have been reported to be closely involved in endocytosis and autophagy through maintaining normal lysosomal function (30-33). Our study showed, for the first time, that in the later stage of endocytosis and autophagy, ATP6V0E2 plays an important role for the fusion of lysosome with endosome or autophagosome. Furthermore, a normal lysosomal function and autophagic flux in macrophages enable the degradation of ox-LDL and thereby decreases the formation of foam cells (7). In oxLDL-loaded *LDLR* KO macrophages, the formation of autophagosome was intact as indicated by the similar expression levels of ATG5, whereas an increased

expressions of LC3 II and P62 in *LDLR* KO compared to *ALDH2/LDLR* DKO signaled a decreased autophagic flux due to an impaired lysosomal function caused by decreased expression of ATP6V0E2 (Figure 3B). Intriguingly, however, ALDH2 deficiency alone appears to decrease autophagic flux without affecting endocytosis compared to WT (Supplemental Figure S5B and S5C), suggesting other unknown mechanisms are most likely involved in autophagic regulation in the presence of LDLR. Lastly, it remains to be studied how AMPK-phosphorylated ALDH2 is translocated into nucleus. We performed a preliminary proteomic study on ALDH2-immunoprecipitated nuclear fraction of *LDLR* KO BMDMs treated with Metformin and identified a list of interacting proteins with ALDH2 in the nucleus. Among them, DDX5, known as P68, was reported as a shuttle between the nucleus and the cytoplasm, consistent with the function of the protein in transcriptional regulation and pre-mRNA splicing (data not shown) (34). These data suggest that ALDH2 is likely translocated to the nucleus by binding to nuclear transporters, such as P68.

AMPK is a key factor that enables the nuclear translocation of ALDH2 in the absence of LDLR or ALDH2 rs671 mutant. The role of AMPK in CVD has been wide recognized, including suppressing inflammatory signaling, monocyte differentiation, and foam cell formation (35). Our data presented here strongly support the notion that AMPK plays an important role in regulating macrophages metabolism of ox-LDL through phosphorylating ALDH2. AMPK activators, Metformin and AICAR, inhibited monocyte-to-macrophage differentiation through AMPK-mediated inhibition of STAT3 activation (36). Ma et al demonstrated that ALDH2 exerted cardio-protection against myocardial I/R injury through an AMPK-dependent induction of autophagy during ischemia and a paradoxical Akt-dependent reduction in autophagy during reperfusion (37). This elegant study appeared to suggest a role of detoxification of toxic aldehydes in ALDH2-elicited regulation of AMPK and AKT pathway *via* LKB1 and PTEN signaling. Intriguingly, however, the regulation of AMPK in macrophages appears to be different from cardiomyocytes in which we did not observe the alteration of the upstream kinases of AMPK (Figure S9A). The discrepancy in mouse phenotypes between APOE and

LDLR background prompted us to study the unknown role of LDLR in the binding of ALDH2 and AMPK. Data shown in Figure 5 and Figure 6 strongly supported a direct protein-protein interaction of AMPK and ALDH2, which is important in regulating lysosome function and autophagy in macrophage.

ALDH2 SNP rs671, the inactive *ALDH2*2* variant (E487K), affects around 40% of East Asians. This *ALDH2* SNP has been associated with increased CVDs, such as heart failure and stroke (38), and gastrointestinal cancers (39). However, previous studies have exclusively focused on the role of alcohol consumptions; it remains elusive whether other molecular mechanisms are involved in diseases associated with this SNP. Our data clearly showed that SNP rs671 mutant attenuated the binding of ALDH2 to LDLR and increased the binding to AMPK, which enables more mutant ALDH2 translocate into nucleus to suppress the expression of *ATP6V0E2* and cause impaired lysosomal function and autophagy. The net outcome of these effects is an excessive accumulation of oxidized LDL and enhanced foam cell formation. The molecular mechanism identified in current study raises an interesting concern that activation of AMPK by the widely used antidiabetic drug Metformin may potentially exert increased risk in atherosclerosis for humans with ALDH2 SNP rs671. Even though significant amount of data support Metformin as protective against CVD, it remains to be studied in the patients with ALDH2 SNP rs671.

In conclusion, our study discovered a new pathway through which *ALDH2* rs671 SNP promotes macrophage foam cell formation in atherosclerosis by attenuating the interaction with LDLR but increasing the interaction with AMPK to promote the translocation of ALDH2 into nucleus to suppress the transcription of *ATP6V0E2*, thereby impairing a lysosomal function in macrophages. This finding represents a novel molecular mechanism by which *ALDH2* rs671 carriers are prone to CVDs, implying that AMPK activation increases atherosclerosis for humans with *ALDH2* rs671 mutant.

Methods

Animals. Mice were housed in a pathogen-free, temperature/light-controlled animal facility under a 12-hour light/dark cycle. *ALDH2*$^{-/-}$*LDLR*$^{-/-}$ mice were obtained by crossing *ALDH2*$^{-/-}$ mice (a gift from Drs. Jun Ren and Aijun Sun, Zhongshan Hospital affiliated with Fudan University, Shanghai, China) (37) (40) and *LDLR* $^{-/-}$ mice (Jackson Laboratory, Bar Harbor, ME). *ALDH2*$^{-/-}$*APOE*$^{-/-}$ mice were obtained by crossing *ALDH2*$^{-/-}$ mice and *APOE* $^{-/-}$ mice （purchased from Shanghai Model Organisms). All mice used in present studies were on a C57BL/6 background. For atherosclerotic study, 6 weeks-old mice were fed Western Diet (Catalog No. D12079B, Research Diets, New Brunswick, NJ) for 12 weeks or 26 weeks (26 weeks were replicated). The numbers of mice studied in each experiment were shown in figure legends.

Cell culture. HEK 293T cell lines were purchased from the CAS Cell Bank and cultured in DMEM containing 10% FBS. Isolation of Bone Marrow-Derived Macrophages (BMDMs) followed a previously published protocol (41). All BMDMs or human macrophages for detecting autophagy were pretreated with 50ug/mL ox-LDL.

Cholesterol depletion. To deplete cholesterol, BMDMs were treated with 1640 supplemented with 5% lipoprotein-deficient serum (LPDS), 1 μM lovastatin, and 10 μM mevalonate for 16h.

Bone Marrow Transplant (BMT). BMT experiments were performed according to a published protocol (42). After recovery, chimeric mice were fed western diet for 12 weeks.

Analysis of Aortic Lesions. A previous published protocol was followed to analyze aortic lesions (43).

Histology and Immunohistochemistry (IHC). The mice hearts were fixed with 4% formaldehyde overnight at 4°C and embedded in paraffin. Then, the heart samples were sectioned into 8μm sections from the brachiocephalic trunk through the aortic root. These sections were then stained with Masson blue for collagen components and IHC staining was used to analyze macrophages and α-SMCs with specific primary antibodies and corresponding secondary antibodies (ZSGB-BIO, China). For IHC, the sections were washed with dimethylbenzene twice for 15 mins, ethanol twice for 5 mins, 95% ethanol for 5 mins, 70% ethanol for 5 mins, ddH2O twice for 5mins and PBS for 5mins. Next, antigen retrieval was conducted by using 10mM sodium citrate. Slides in sodium citrate were boiled three times for 2 mins and cooled 2 mins. Then slides were blocked in 10% normal serum with 1% BSA in TBS for 30 mins at room temperature. Then, slides were incubated with specific primary antibodies (anti-CD68 from Catalog No. MCA1957, Bio-Rad, USA or anti-α-SMC-actin from Catalog No. ab5694, Abcam, USA) overnight at 4°C. After recovering to room temperature, slides were incubated with secondary antibody and stained with DAB buffer (Catalog No. ZLI-9017, ZSGB-BIO, China). All sections were analyzed with ImageJ for quantitative measurements.

Phagocytotic Assay. BMDMs were incubated in 37℃ for detecting ox-LDL content or 4℃ for binding with 10 μg/ml Dil-oxLDL (Catalog No. YB-0010, Yiyuan Biotechnologies, China) for 4 hours or 50ug/mL ox-LDL (Catalog No. YB-002, Yiyuan Biotechnologies, China) for 6 hours. Staining and analyzing followed previous reference (41). AICAR (Catalog No. S1802, Selleck, USA) or Bafilomycin-A1 (Catalog No. S1413, Selleck, USA) was added to cell medium to make the final concentrations of 1 mM AICAR and 10 nM Baf-A1, respectively, an hour before adding Dil-oxLDL or ox-LDL.

Western Blotting. SDS-PAGE was used to separate total cell lysate and transferring proteins to PVDF membranes (Millipore, Bedford, MA). The immune-reactive protein bands were

visualized by ECL kit (Proteintech, USA). Antibodies against ALDH2 (Catalog No. 15310-1-AP), LDLR (Catalog No. 10785-1-AP), ATG5 (Catalog No. 10181-2-AP), HDAC1 (Catalog No. 10197-1-AP) ,HDAC2 (Catalog No. 12922-3-AP), HDAC3 (Catalog No. 10255-1-AP) , Lamin B1 (Catalog No. 66095-1-Ig), ACAT1 (Catalog No. 16215-1-AP) , His-Tag (Catalog No. 66005-1-Ig) and GAPDH(Catalog No. 60004-1-Ig) were purchased from Proteintech. Antibodies for P-AMPK (Thr172) (Catalog No.2535S), T-AMPK (Catalog No. 5832T), LC3B (Catalog No.2775S), Myc-Tag (Catalog No.2276S), RAB11 (Catalog No. 5589T), EEA1 (Catalog No. 3288T), RAB7 (Catalog No. 9367T), RAB5 (Catalog No.3547T), LAMP1 (Catalog No. 90917), Clathrin (Catalog No. 4796T) and normal rabbit IgG (Catalog No.2729S) were purchased from Cell Signaling Technology. Antibody for ATP6V0E2 (Catalog No. ab178934), LOX1 (Catalog No.ab60178), H3 (Catalog No.ab4729), P62 (Catalog No. ab91526), SRA (Catalog No. ab183725) were purchased from Abcam (Abcam, USA). ABCA1 (Catalog No. NB400-105) and CD36 (Catalog No. NB400-144SS) were purchansed from Novus. Flag-Tag (Catalog No.F1804) was purchased from Sigma.

Detection of Phosphorylated ALDH2 by using iTRAQ proteomics. 10% SDS-PAGE was used to separate total cell lysate for silver stain (Catalog No. P0017S, Beyotime, China). ALDH2 gel was cut in 53kDa and the phosphorylation of ALDH2 was measured by using iTRAQ- proteomics which was carried out by Shanghai Applied Protein Technology.

ATP, ADP and AMP detection by LC–MS. 10^7 BMDMs with or without 50μg/mL oxLDL treatment were collected by Trypsin-EDTA (Catalog No. 25200056, Gibico). Washed twice by using 1xPBS. BMDMs were pre-treated by following the reference(44). Then, ATP, ADP and AMP levels were detected by following previous reference (45).

Detection of Phosphorylated ALDH2 in SuperSep™Phos-tag™ SDS-PAGE. SuperSep™Phos-tag™ SDS-PAGE (Catalog No.198-17981, Wako, Japan) was used for detection of phosphorylated ALDH2 in BMDMs.

Nuclear and Cytoplasmic Fractionation. Separating the cytoplasmic and nuclear proteins was conducted by using the NE-PER nuclear and cytoplasmic extraction kit (Catalog No. P0027, Beyotime, China) according to the manufacturer's instructions.

Cholesterol Efflux Assay. BMDMs firstly were treated with 15μg/ml chol-d7 for 24h. After washing the cells thoroughly with PBS, 50μg/ml HDL was added to induce cholesterol efflux. After incubating 24h, media were collected for GC-MS and 10% BMDMs proteins were collected for quantification.

BMDMs were treated with 15μg/ml cholesterol-d7 (chol-d7) for 24h. 10% BMDMs were used to measure protein concentration. Free cholesterol was extracted by using 2ml hexane: IPA (3:2, v/v) supplemented with 1% acetic acid and 6μg 5α-cholestane as internal standard (IS). The upper organic phase was dried under nitrogen, 40ul of pyridine and 40ul of derivatizing agent (BSTFA + TMCS) for GC-MS analysis were added. GC-MS was performed in the EI mode using Shimadzu GC-MS QP2010.Then peak areas were integrated using the instrument software. Calibration curves were generated using chol-d7 and IS. The final results were normalized to cell lysates protein.

Hydrolysis of Cholesteryl esters (CE). Macrophages were incubated with 50 μg/mL ox-LDL with or without 5nM Balfmycin-A1 for 20h. CE were extracted by adding 4mL hexane: IPA (3:2, v/v) and 3μg CE 19:0 as an internal standard (IS). The upper organic phase was dried under nitrogen and 50ul of hexane for LC-MS analysis were added. Normal phase LC was carried out with Agilent 1260 Quat pump VL and Accela 1250 pump. The MS was performed on a TSQ Vantage (Thermo Fisher Scientific) in positive ion and multiple reaction monitoring (MRM)

mode. Chromatographic peaks were integrated and area ratios (samples *versus* IS) were generated using Xcalibur (Thermo Scientific, San Jose, USA). CE changes (hydrolysis) were expressed as fold change relative to control, calculated as follow: % hydrolysis = (CE1 – CE2)/(CE1) *100, where CE1 represented CE after treating with ox-LDL for 20h, and CE2 represents CE after the macrophages were incubated for 20 h with 50 μg/mL HDL; fold change = (% hydrolysis sample/% hydrolysis control).

Real-time PCR. BMDMs were lysed with TRIzol reagent (Catalog No.9109, Takara, Japan). RNA was purified and reverse transcribed into cDNA. The genes expression was normalized to *L32* expression. The primer sequences were showed in supplemental **Table 2**. The fold change was calculated by using the comparative ΔCt methods and showed as relative transcript levels.

Retrovirus (TRV). LDLR KO BMDMs were incubated with 5μg/mL polybrene and 100μL $5*10^7$ TU/mL HBhTRV-m-LDLR-3xflag-GFP in 900 μL cell medium (RPMI-1640+10% FBS) at 37 °C for 4 hours. Then, we added 1mL cell medium with 5 μg/mL polybrene. Cell medium was changed after incubating 24 hours at 37 °C and then BMDMs were incubated 48 hours.

Immunoprecipitation (IP). For BMDMs, target protein was precipitated with respective antibodies and protein A/G beads (catalog no. B23202, Biotool, USA). For 293T cells, cells transfected with specifically tagged protein by using Attractene Transfection Reagent (Catalog No. 301005, Qiagen, Germany) was lysed and incubated with myc-beads or flag-beads (Catalog No. B26301 for myc-beads, Catalog No. B23102 for flag-beads, Biotool, USA).

Fluorescence Microscopy. BMDMs were grown on glass coverslips in 6-well dishes. Immunofluorescence staining was followed by previous reference (42). Percent of ALDH2

translocation is calculated according to areas of ALDH2 signal in nucleus /nucleus area (quantified by Image J).

RNA-Seq Analysis. BMDMs were lysed with TRIzol reagent. The library preparation and sequencing were carried out by Beijing Genomics Institute BGI (Wuhan, China). We measured the expression of the transcripts isoforms by using RSEM and used NOISeq method to screen differentially expressed genes (DEGs) between two groups. Top 3 GO functional classifications on overlapping DEGs showed in supplemental **Table 3.** Heat maps were conducted by using the R software. Microarray data were deposited in the Gene Expression Omnibus with the accession number GSE121310.

Chromatin Immunoprecipitation (ChIP Assay). BMDMs cultured in 10cm plates were pretreated with or without 1mM AICAR for 1 h. ChIP assay was conducted by using ChIP Assay kit (Catalog No. 17-295, Millipore, USA). Eluted DNA was further purified using PCR purification kit (Qiagen).

Detection of Autophagic Flux. BMDMs were plated and grew overnight on 20 mm glass bottom cell culture dish (Catalog No.801001, NEST, USA). The formation of autolysosomes in BMDMs in control and Bafilomycin A1 (1nM), Chloroquine (10μM), Leupeptin (100μM) treated cells was detected using the PremoTM Autophagy Tandem Sensor RFP-GFP-LC3B Kit (Catalog No. P36239, Thermo Fischer Scientific, USA). Fluorescent images were taken by using confocal microscopy (Carl Zeiss Meditec, Inc.) and quantified by using Image J software. Quantified mean number of autolysosomes per cell is according to the dots of RFP signal in the merge picture.

Luciferase Assay. 293T cells were transfected with pGL3.1/pCMV-*ATP6V0E2* (20:1) for 24h. Luciferase activity was measured by using the Dual Luciferase Reporter Assay System (Catalog No. E1960, Promega, USA). The GL (firefly luciferase) activity was normalized to co-

expressed RL (renilla luciferase) activity. 293T cells were transfected with Lipofectamine® 2000 Reagent (Cat No.1854311, Invitrogen, USA).

Human Macrophages. Human monocytes were isolated from peripheral blood mononuclear cells (PBMC). Peripheral blood mononuclear cells (PBMCs) were isolated by using a Ficoll (Catalog No.17-1440-02, BD) density gradient, and then were isolated from PBMCs by using anti-CD14 magnetic beads (Catalog No. 11149D, Thermo) according to the manufacturer's protocol. Then, human monocytes were differentiated into human macrophages by treatment with differentiated medium (1640+5%AB human serum+10%FBS+PS+25 ng/ml M-CSF) 7 days.

Plasmids. Flag-tagged human ALDH2, ALDH2 (rs671) mutant clone, Myc and 6xHis tagged Human LDLR were constructed into pcDNA3.0 vector. Clones were picked and amplified to be sequenced to verify the final results.

Statistical Analysis. Results were expressed as mean ± SD or mean ± SEM from at least three independent experiments by using GraphPad Prism 5. Statistical analysis was conducted by using an unpaired Student's t test or two-way ANOVA. A two-tailed probability value of < 0.05 was considered statistically significant. *$p < 0.05$; **$p < 0.01$; ***$p < 0.001$.

Study Approval. All animal experiments were approved by the Institutional Animal Care and Use Committee of the SIBS, CAS, Shanghai, China (Approval Number: 2015-AN-2). All human samples were collected by Shanghai General Hospital and human experiments were approved by Ethics Committee of Shanghai General Hospital affiliated with Shanghai Jiao Tong University School of Medicine, Shanghai, China.

Author contributions

HYY and SSZ designed the research studies and experiments. SSZ carried out a majority of the experiments. LXL helped perform experiments in bone marrow transplant and measuring aorta lesions. YLZ and LLZ helped the clinical study. JHL and SYG developed and the LC-MS method and helped measuring cholesterol esters and cholesterol efflux. NNL performed experiments in primary culture of BMDMs. JG performed RNA-seq analysis. MJZ performed phosphoproteomics data analysis. YZT developed GC/MS method and helped detecting cholesterol. YCW and HYY designed the clinical study. HYY and SSZ wrote and approved this manuscript.

Acknowledgements

The authors would like to acknowledge Drs. Jun Ren and Aijun Sun from Shanghai Institute of Cardiovascular Diseases, Zhongshan Hospital affiliated with Fudan University, Shanghai, China, for providing *ALDH2*$^{-/-}$ mice. We acknowledge the help from Mr. Zhimin Hu at SIBS in bone marrow transplant experiments. A constructive discussion with Dr. Dawei Zhang at University of Alberta, Canada, and Dr. Ming-Hui Zou from Georgia State University, USA, Dr. Bao-liang Song from Wuhan University, China, is also greatly appreciated.

Sources of Funding

This work was financially supported by National Natural Science Foundation of China (31470831, 91439103, 91539127, and 31401015) and the National Key R&D Program of China administered by Chinese Ministry of Science and Technology (MOST) (2016YFD0400205, 2016YFC0903403) and a grant from the Chinese Academy of Sciences (ZDBS-SSW-DQC-02).

Reference:

1. Weber C, and Noels H. Atherosclerosis: current pathogenesis and therapeutic options. *Nat Med.* 2011;17(11):1410-22.
2. Moore Kathryn J, and Tabas I. Macrophages in the Pathogenesis of Atherosclerosis. *Cell.*

2011;145(3):341-55.

3. Zhao B, Song J, Chow WN, St Clair RW, Rudel LL, and Ghosh S. Macrophage-specific transgenic expression of cholesteryl ester hydrolase significantly reduces atherosclerosis and lesion necrosis in Ldlr mice. *J Clin Invest.* 2007;117(10):2983-92.
4. Ouimet M, Ediriweera H, Afonso MS, Ramkhelawon B, Singaravelu R, Liao X, Bandler RC, Rahman K, Fisher EA, Rayner KJ, et al. microRNA-33 Regulates Macrophage Autophagy in Atherosclerosis. *Arterioscler Thromb Vasc Biol.* 2017;37(6):1058-67.
5. Sergin I, Evans TD, and Razani B. Degradation and beyond: the macrophage lysosome as a nexus for nutrient sensing and processing in atherosclerosis. *Curr Opin Lipidol.* 2015;26(5):394-404.
6. Ouimet M, Franklin V, Mak E, Liao X, Tabas I, and Marcel YL. Autophagy regulates cholesterol efflux from macrophage foam cells via lysosomal acid lipase. *Cell Metab.* 2011;13(6):655-67.
7. Sergin I, Evans TD, Zhang X, Bhattacharya S, Stokes CJ, Song E, Ali S, Dehestani B, Holloway KB, Micevych PS, et al. Exploiting macrophage autophagy-lysosomal biogenesis as a therapy for atherosclerosis. *Nat Commun.* 2017;8(15750.
8. Getz GS, and Reardon CA. Do the Apoe-/- and Ldlr-/- Mice Yield the Same Insight on Atherogenesis? *Arterioscler Thromb Vasc Biol.* 2016;36(9):1734-41.
9. Defesche JC, Gidding SS, Harada-Shiba M, Hegele RA, Santos RD, and Wierzbicki AS. Familial hypercholesterolaemia. *Nat Rev Dis Primers.* 2017;3(17093.
10. Somanathan S, Jacobs F, Wang Q, Hanlon AL, Wilson JM, and Rader DJ. AAV vectors expressing LDLR gain-of-function variants demonstrate increased efficacy in mouse models of familial hypercholesterolemia. *Circ Res.* 2014;115(6):591-9.
11. Ishibashi S, Brown MS, Goldstein JL, Gerard RD, Hammer RE, and Herz J. Hypercholesterolemia in low density lipoprotein receptor knockout mice and its reversal by adenovirus-mediated gene delivery. *J Clin Invest.* 1993;92(2):883-93.
12. Piedrahita JA, Zhang SH, Hagaman JR, Oliver PM, and Maeda N. Generation of mice carrying a mutant apolipoprotein E gene inactivated by gene targeting in embryonic stem cells. *Proc Natl Acad Sci U S A.* 1992;89(10):4471-5.
13. Pradhan AD, Aday AW, Rose LM, and Ridker PM. Residual Inflammatory Risk on Treatment With PCSK9 Inhibition and Statin Therapy. *Circulation.* 2018;138(2):141-9.
14. Raal FJ, Honarpour N, Blom DJ, Hovingh GK, Xu F, Scott R, Wasserman SM, and Stein EA.

Inhibition of PCSK9 with evolocumab in homozygous familial hypercholesterolaemia (TESLA Part B): a randomised, double-blind, placebo-controlled trial. *The Lancet.*385(9965):341-50.

15. Chen CH, Sun L, and Mochly-Rosen D. Mitochondrial aldehyde dehydrogenase and cardiac diseases. *Cardiovasc Res.* 2010;88(1):51-7.
16. Guo JM, Liu AJ, Zang P, Dong WZ, Ying L, Wang W, Xu P, Song XR, Cai J, Zhang SQ, et al. ALDH2 protects against stroke by clearing 4-HNE. *Cell Res.* 2013;23(7):915-30.
17. Pan C, Xing JH, Zhang C, Zhang YM, Zhang LT, Wei SJ, Zhang MX, Wang XP, Yuan QH, Xue L, et al. Aldehyde dehydrogenase 2 inhibits inflammatory response and regulates atherosclerotic plaque. *Oncotarget.* 2016;7(24):35562-76.
18. Crabb DW, Edenberg HJ, Bosron WF, and Li TK. Genotypes for aldehyde dehydrogenase deficiency and alcohol sensitivity. The inactive ALDH2(2) allele is dominant. *J Clin Invest.* 1989;83(1):314-6.
19. Xiao Q, Weiner H, and Crabb DW. The mutation in the mitochondrial aldehyde dehydrogenase (ALDH2) gene responsible for alcohol-induced flushing increases turnover of the enzyme tetramers in a dominant fashion. *J Clin Invest.* 1996;98(9):2027-32.
20. Han H, Wang H, Yin Z, Jiang H, Fang M, and Han J. Association of genetic polymorphisms in ADH and ALDH2 with risk of coronary artery disease and myocardial infarction: a meta-analysis. *Gene.* 2013;526(2):134-41.
21. Choi JW, Kim JH, Cho SC, Ha MK, Song KY, Youn HD, and Park SC. Malondialdehyde inhibits an AMPK-mediated nuclear translocation and repression activity of ALDH2 in transcription. *Biochem Biophys Res Commun.* 2011;404(1):400-6.
22. Tang WHW, and Hazen SL. Atherosclerosis in 2016: Advances in new therapeutic targets for atherosclerosis. *Nat Rev Cardiol.* 2017;14(2):71-2.
23. Li H, Borinskaya S, Yoshimura K, Kal'ina N, Marusin A, Stepanov VA, Qin Z, Khaliq S, Lee MY, Yang Y, et al. Refined geographic distribution of the oriental ALDH2*504Lys (nee 487Lys) variant. *Ann Hum Genet.* 2009;73(Pt 3):335-45.
24. Gomes KM, Campos JC, Bechara LR, Queliconi B, Lima VM, Disatnik MH, Magno P, Chen CH, Brum PC, Kowaltowski AJ, et al. Aldehyde dehydrogenase 2 activation in heart failure restores mitochondrial function and improves ventricular function and remodelling. *Cardiovasc Res.* 2014;103(4):498-508.
25. Zhao X, Hua Y, Chen H, Yang H, Zhang T, Huang G, Fan H, Tan Z, Huang X, Liu B, et al. Aldehyde dehydrogenase-2 protects against myocardial infarction-related cardiac fibrosis

through modulation of the Wnt/β-catenin signaling pathway. *Therapeutics and Clinical Risk Management.* 2015;11(1371-81.

26. Yun KE, Chang Y, Yun SC, Davey Smith G, Ryu S, Cho SI, Chung EC, Shin H, and Khang YH. Alcohol and coronary artery calcification: an investigation using alcohol flushing as an instrumental variable. *Int J Epidemiol.* 2017;46(3):950-62.
27. Chan L, Hong J, Pan J, Li J, Wen Z, Shi H, Ding J, and Luo X. Role of Rab5 in the formation of macrophage-derived foam cell. *Lipids Health Dis.* 2017;16(1):170.
28. Chistiakov DA, Melnichenko AA, Myasoedova VA, Grechko AV, and Orekhov AN. Mechanisms of foam cell formation in atherosclerosis. *J Mol Med (Berl).* 2017.
29. Hohn A, Sittig A, Jung T, Grimm S, and Grune T. Lipofuscin is formed independently of macroautophagy and lysosomal activity in stress-induced prematurely senescent human fibroblasts. *Free Radic Biol Med.* 2012;53(9):1760-9.
30. Mijaljica D, Prescott M, and Devenish RJ. V-ATPase engagement in autophagic processes. *Autophagy.* 2011;7(6):666-8.
31. Florey O, Gammoh N, Kim SE, Jiang X, and Overholtzer M. V-ATPase and osmotic imbalances activate endolysosomal LC3 lipidation. *Autophagy.* 2015;11(1):88-99.
32. Forgac M, Cantley L, Wiedenmann B, Altstiel L, and Branton D. Clathrin-coated vesicles contain an ATP-dependent proton pump. *Proc Natl Acad Sci U S A.* 1983;80(5):1300-3.
33. Blake-Palmer KG, Su Y, Smith AN, and Karet FE. Molecular cloning and characterization of a novel form of the human vacuolar H+-ATPase e-subunit: An essential proton pump component. *Gene.* 2007;393(1):94-100.
34. Wang H, Gao X, Huang Y, Yang J, and Liu ZR. P68 RNA helicase is a nucleocytoplasmic shuttling protein. *Cell Res.* 2009;19(12):1388-400.
35. Salt IP, and Hardie DG. AMP-Activated Protein Kinase: An Ubiquitous Signaling Pathway With Key Roles in the Cardiovascular System. *Circ Res.* 2017;120(11):1825-41.
36. Vasamsetti SB, Karnewar S, Kanugula AK, Thatipai AR, Kumar JM, and Kotamraju S. Metformin Inhibits Monocyte-to-Macrophage Differentiation via AMPK-Mediated Inhibition of STAT3 Activation: Potential Role in Atherosclerosis. *Diabetes.* 2015;64(6):2028-41.
37. Ma H, Guo R, Yu L, Zhang Y, and Ren J. Aldehyde dehydrogenase 2 (ALDH2) rescues myocardial ischaemia/reperfusion injury: role of autophagy paradox and toxic aldehyde. *Eur Heart J.* 2011;32(8):1025-38.
38. Cai Q, Wu J, Cai Q, Chen EZ, and Jiang ZY. Association between Glu504Lys polymorphism

of ALDH2 gene and cancer risk: a meta-analysis. *PLoS One.* 2015;10(2):e0117173.

39. Jin S, Chen J, Chen L, Histen G, Lin Z, Gross S, Hixon J, Chen Y, Kung C, Chen Y, et al. ALDH2(E487K) mutation increases protein turnover and promotes murine hepatocarcinogenesis. *Proc Natl Acad Sci U S A.* 2015;112(29):9088-93.
40. Sun A, and Ren J. ALDH2, a novel protector against stroke? *Cell Res.* 2013;23(7):874-5.
41. Lu J, Guo S, Xue X, Chen Q, Ge J, Zhuo Y, Zhong H, Chen B, Zhao M, Han W, et al. Identification of a novel series of anti-inflammatory and anti-oxidative phospholipid oxidation products containing the cyclopentenone moiety in vitro and in vivo: Implication in atherosclerosis. *J Biol Chem.* 2017;292(13):5378-91.
42. Tang J, Shen Y, Chen G, Wan Q, Wang K, Zhang J, Qin J, Liu G, Zuo S, Tao B, et al. Activation of E-prostanoid 3 receptor in macrophages facilitates cardiac healing after myocardial infarction. *Nat Commun.* 2017;8(14656.
43. Yan S, Tang J, Zhang Y, Wang Y, Zuo S, Shen Y, Zhang Q, Chen D, Yu Y, Wang K, et al. Prostaglandin E2 promotes hepatic bile acid synthesis by an E prostanoid receptor 3-mediated hepatocyte nuclear receptor 4alpha/cholesterol 7alpha-hydroxylase pathway in mice. *Hepatology.* 2017;65(3):999-1014.
44. Yuan M, Breitkopf SB, Yang X, and Asara JM. A positive/negative ion-switching, targeted mass spectrometry-based metabolomics platform for bodily fluids, cells, and fresh and fixed tissue. *Nat Protoc.* 2012;7(5):872-81.
45. Zhang CS, Hawley SA, Zong Y, Li M, Wang Z, Gray A, Ma T, Cui J, Feng JW, Zhu M, et al. Fructose-1,6-bisphosphate and aldolase mediate glucose sensing by AMPK. *Nature.* 2017;548(7665):112-6.

Figure 1

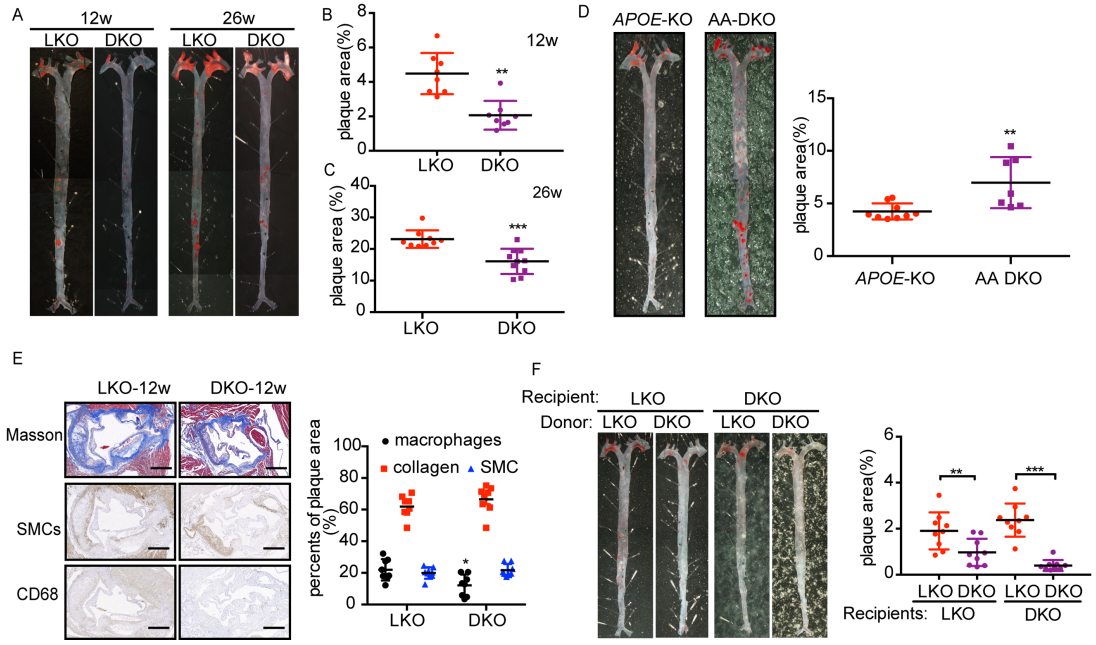

Figure 1. ALDH2 knockout decreases areas of atherosclerotic plaque in *LDLR* KO background mice but increases areas of atherosclerotic plaque in *APOE* KO background mice. A, Representative *en face* Sudan IV staining; **B to C,** quantification of plaque areas of aortas from male 12w WD (n=8, B) and 26w of WD (n=9-10, C, conducted twice)**. D,** representative en face Sudan IV staining (n=7-9) and quantification of Sudan IV-positive areas of aortas from male mice after 12w WD feeding *APOE* KO and *APOE/ALDH2* DKO (AA-DKO) mice. **E,** representative IHC and quantification of macrophages, collagen, and SMC after 12 weeks of WD feeding (n=8). Scale bar, 400μm. **F,** representative *en face* Sudan IV staining and quantification of Sudan IV-positive areas of aortas from male *LDLR* KO mice (left, n=9) and *LDLR/ALDH2* DKO mice (right, n=9) transplanted by *LDLR* KO and *ALDH2/LDLR* DKO bone marrow**.** Statistical comparisons were made using 2-tailed Student's t test. All data represent mean ± SD.*P < 0.05, **P < 0.01, ***P < 0.001.

Figure 2

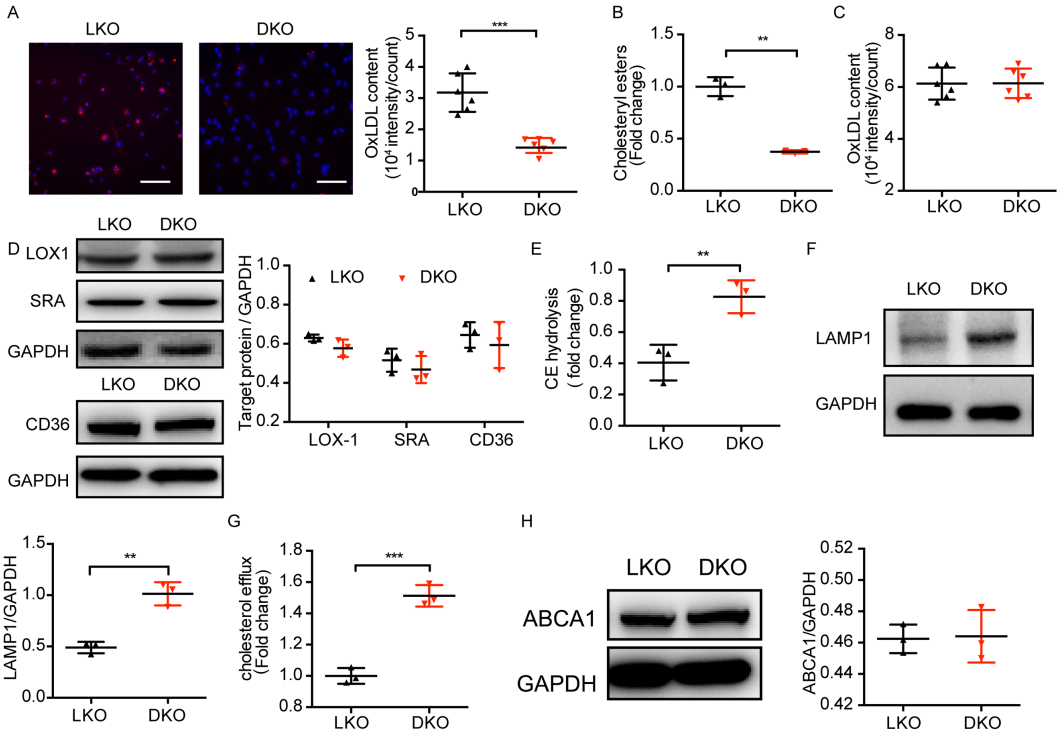

Figure 2. *ALDH2/LDLR* DKO macrophages exhibit decreased foam cells compared to LKO through restoring the lysosomal function and increased CE hydrolysis without affecting oxLDL binding and ABCA1 expression. A, *ALDH2* KO decreases foam cell formation in *LDLR* KO (LKO) BMDMs and quantification (n=6). The oxLDL signals are shown in red and Hoechst signals are shown in blue. Scale bar, 100 μm. **B,** CE decreased in *ALDH2/LDLR* DKO (DKO) BMDMs comparing to LKO macrophages (n=3). **C,** binding to ox-LDL in LKO and *ALDH2/LDLR* DKO BMDMs (n=6). **D,** expressions of LOX1, SRA, and CD36 in LKO and *ALDH2/LDLR* DKO BMDMs (n=3). **E,** CE hydrolysis significantly increased in *ALDH2/LDLR* DKO BMDMs comparing with LKO macrophages (n=3). **F,** expression of lysosome function marker LAMP1 in macrophages of *LDLR* KO and *ALDH2/LDLR* DKO macrophages (n=3). **G,** cholesterol efflux increased by *ALDH2* KO in *LDLR* KO BMDMs (n=3). **H,** ABCA1 expression in LKO and DKO BMDMs (n=3). Statistical comparisons were made using 2-tailed Student's t test. All data represent mean ± SD. **P < 0.01, ***P < 0.001.

Figure 3

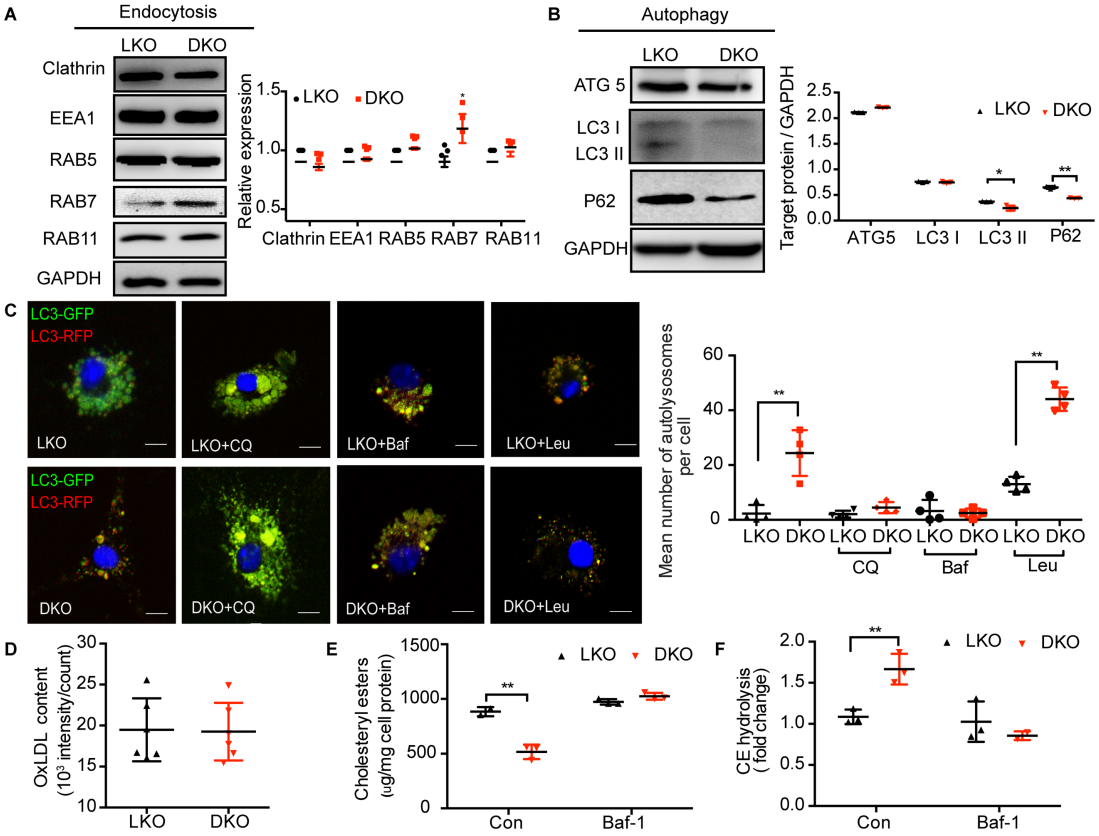

Figure 3. *LDLR/ALDH2* DKO leads to increased macrophage endocytosis, autophagy, and CE hydrolysis in lysosome comparing to *LDLR* KO. A to B, endocytosis (A) and autophagy (B) are increased in *ALDH2/LDLR* DKO macrophages comparing to LKO (n=3). **C,** the number of autolysosome is increased in *ALDH2/LDLR* DKO macrophages comparing to LKO (n=4). **D to F,** inhibition of autophagy by bafilomycin A1 treatment diminishes increased foam cell formation (D, n=6) and cholesterol ester accumulation (E, n=3) due to impaired CE hydrolysis (F, n=3) in LKO macrophages compared to those from DKO. Statistical comparisons were made using 2-tailed Student's t test. All data represent mean ± SD.*P < 0.05, **P < 0.01.

Figure 4

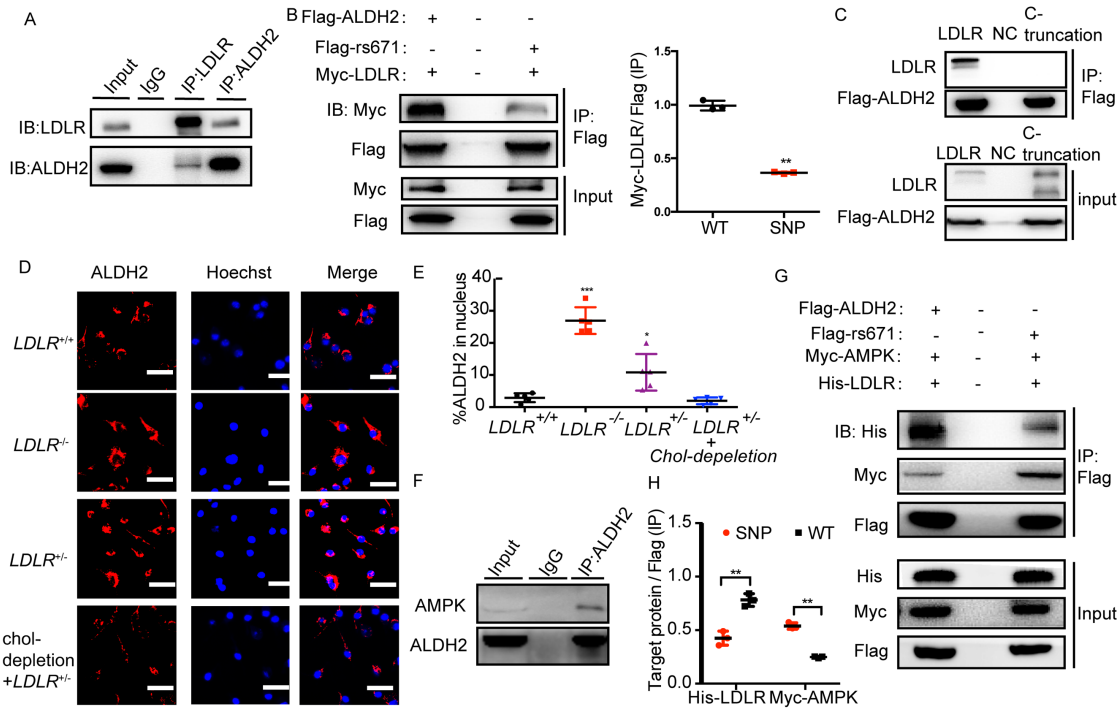

Figure 4. LDLR inhibits but ALDH2 rs671 mutant increases nuclear translocation of ALDH2 through interactions with AMPK. A, LDLR directly interacts with ALDH2 in BMDMs (n=3). **B,** ALDH2 rs671 mutant pulls down much less LDLR compared to WT ALDH2 (n=3). **C,** ALDH2 does not bind to LDLR when LDLR C-terminal is truncated (n=3). **D to E,** LDLR gene-dose dependent inhibition of ALDH2 translocation; LDLR upregulation decreased ALDH2 translocation by cholesterol depletion and quantification (E, n=5)**.** Scale bar, 100 μm. **F,** ALDH2 directly binds to AMPK in *LDLR* KO BMDMs. G **to H,** ALDH2 rs671 mutant pulls down more AMPK compared to WT ALDH2 by co-transfection of Flag-tagged ALDH2, Myc-tagged AMPK and His-tagged LDLR (G) and quantification (H, n=3). Statistical comparisons were made using 2-tailed Student's t test (B and H) or ANOVA (E). All data represent mean ± SD.*P < 0.05, **P < 0.01, ***P < 0.001.

Figure 5

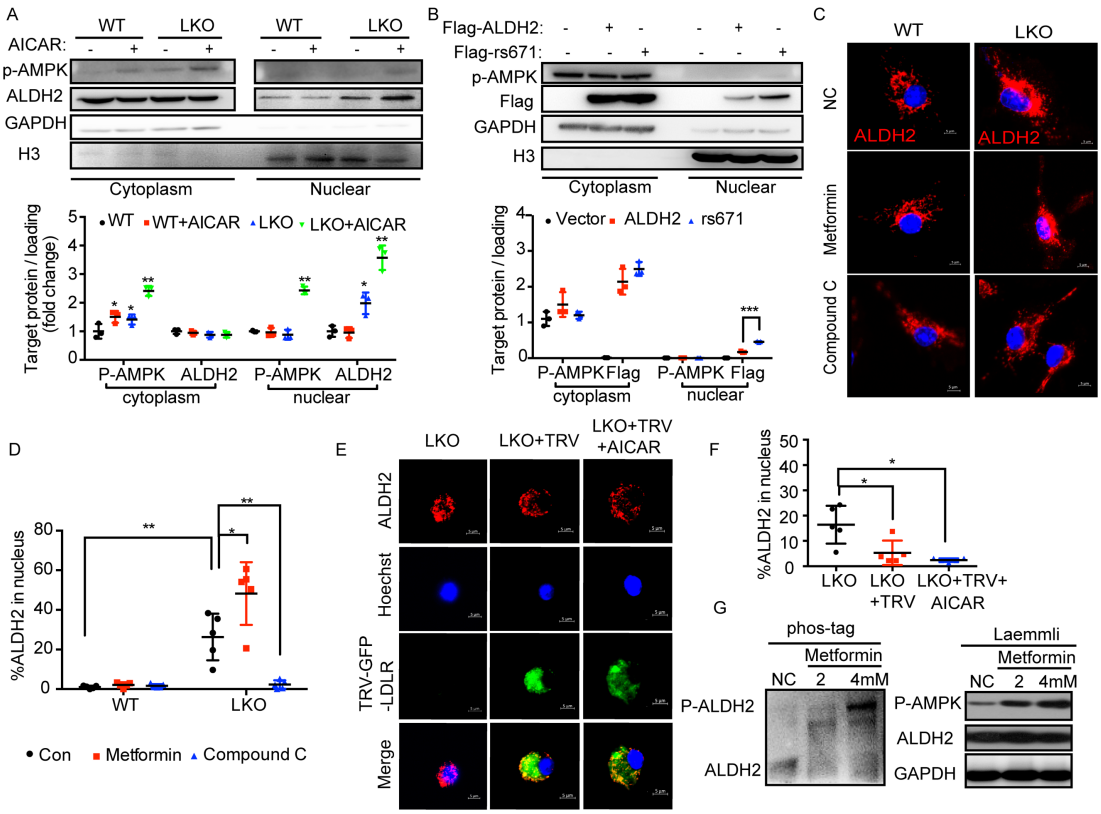

Figure 5. AMPK phosphorylates ALDH2 and promotes ALDH2 translocation in the absence of LDLR or ALDH2 rs671 mutant. A, AMPK activation promotes ALDH2 nuclear translocation in LDLR KO BMDMs by cellular fractionation (n=3). **B,** ALDH2 rs671 mutant increases the translocation of ALDH2 in 293T cell (n=3). **C to D,** AMPK activation leads to ALDH2 nuclear translocation, whereas inhibition of AMPK blocks nuclear translocation of ALDH2, Scale bar, 5 μm (C) and quantification (D, n=5). **E to F,** LDLR blocks the translocation of ALDH2 even AMPK activation (E) and quantification (F, n=5). **G,** AMPK activation leads to a dose-dependent increase of ALDH2 phosphorylation in the absence of LDLR in LKO macrophages by SuperSep^{TM} Phos-tag^{TM} SDS-PAGE. Statistical comparisons were made using ANOVA. All data represent mean ± SD.*P < 0.05, **P < 0.01, ***P < 0.001.

Figure 6

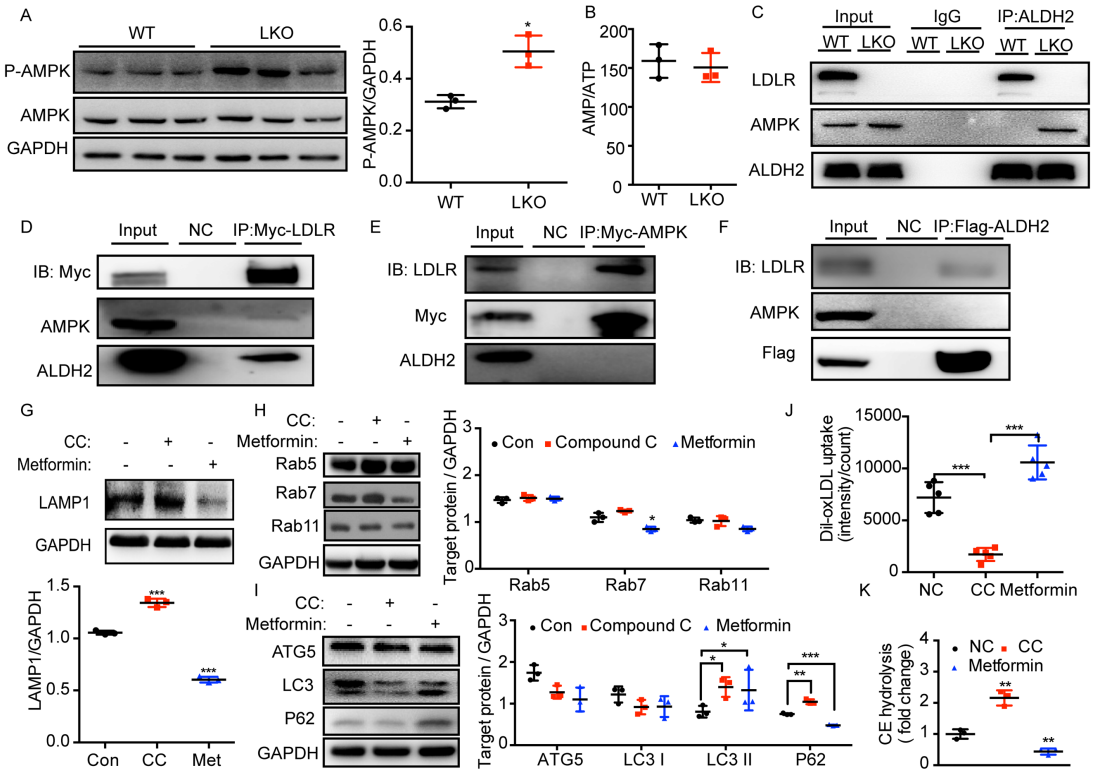

Figure 6. AMPK regulates lysosomal function, endocytosis, autophagy, and foam cell formation in an LDLR-dependent manner. A, LDLR KO increases the AMPK activation in BMDMs (n=3). **B,** Ratio of AMP/ATP in macrophages from *LDLR* KO and WT treated with oxLDL (n=3). **C,** LDLR inhibits the binding of ALDH2 and AMPK in macrophages. **D to F,** AMPK and ALDH2 prefer to bind to LDLR: LDLR pulls down AMPK and ALDH2 (D); AMPK pulls down LDLR but not ALDH2 (E); ALDH2 pulls down LDLR but not AMPK (F). **G,** AMPK activation by Metformin decreases LAMP1 expression, whereas AMPK inhibition by compound C leads to increased LAMP1 expression in LKO BMDMs (n=3). **H to I,** AMPK activation by Metformin decreases endocytosis (H) and autophagy (I), whereas AMPK inhibition by compound C leads to increased endocytosis (H) and autophagy (I) in LKO BMDMs (n=3). **J,** AMPK activation leads to increased foam cell formation, whereas AMPK inhibition results in decreased foam cell formation (n=5). **K,** AMPK activation decreases CE hydrolysis, whereas AMPK inhibition increases CE hydrolysis (n=3). Statistical comparisons were made using 2-tailed Student's t test (A and B) or ANOVA (G, H to K). All data represent mean ± SD.*P < 0.05, **P < 0.01, ***P < 0.001.

Figure 7

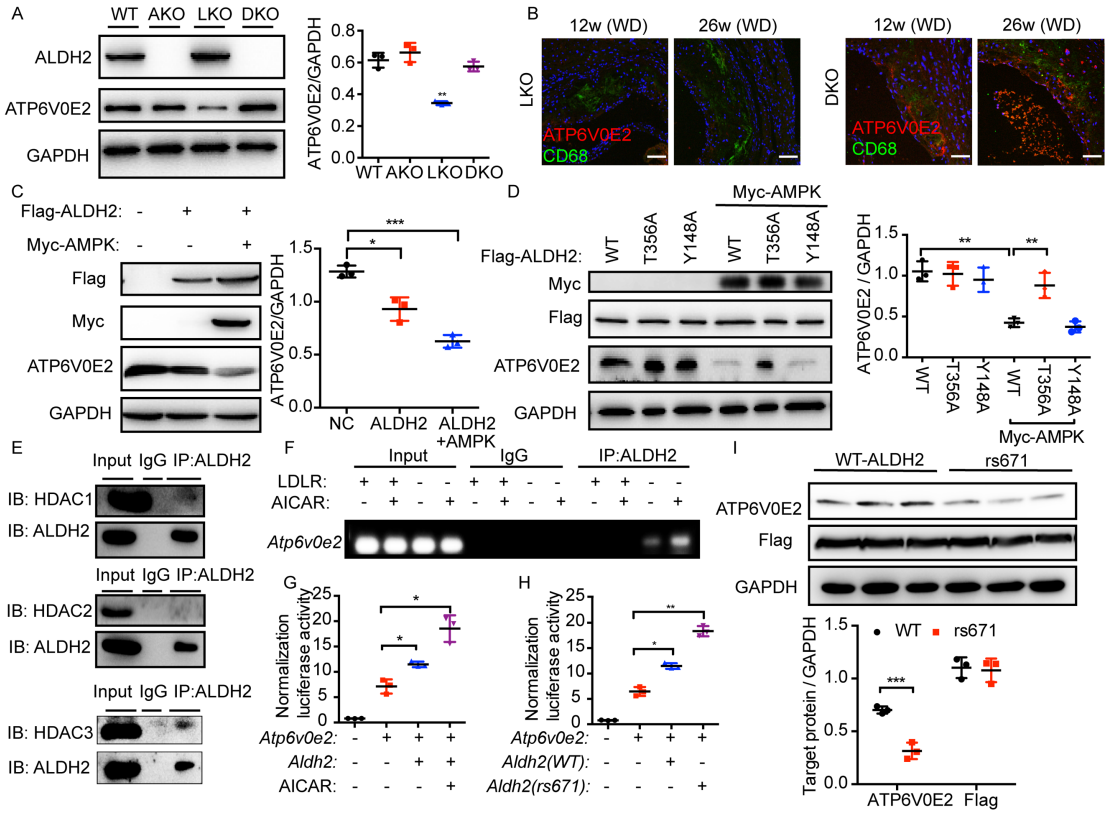

Figure 7. Nuclear translocated ALDH2 regulates the transcription of *ATP6V0E2*, a critical protein for lysosomal function, endocytosis, and autophagy; ALDH2 rs671 polymorphism decreases ATP6V0E2 expression. A, *ALDH2/LDLR* DKO leads to significant upregulation of ATP6V0E2 expression compared to LKO (n=3). **B,** ATP6V0E2 (red) co-localizes with macrophages (CD68, green) and ATP6V0E2 expression is significantly increased in the aorta of DKO mice. Scale bar, 100 μm. **C,** overexpressed AMPK and ALDH2 decrease ATP6V0E2 expression in 293T cells (n=3). **D,** ALDH2 T356A not Y148A mutant rescues decreased ATP6V0E2 expression which is caused by overexpressed ALDH2 and AMPK (n=3). **E,** nuclear translocated ALDH2 binds to HDAC3. **F to G**, nuclear translocated ALDH2 regulates transcription of *ATP6V0E2*: in the absence of LDLR, nuclear translocated ALDH2 binds to *ATP6V0E2* promoter (F) and regulates the transcriptional activity (G), which is enhanced by AMPK activation (n=3). **H,** ALDH2 rs671 enhanced transcriptional activity of ATP6V0E2. **I,** rs671 mutant decreased ATP6V0E2 protein expression (n=3). Statistical comparisons were made using 2-tailed Student's t test (I) or ANOVA (A, C, D, G, and H). All data represent mean ± SD.*P < 0.05, **P < 0.01, ***P < 0.001.

Figure 8

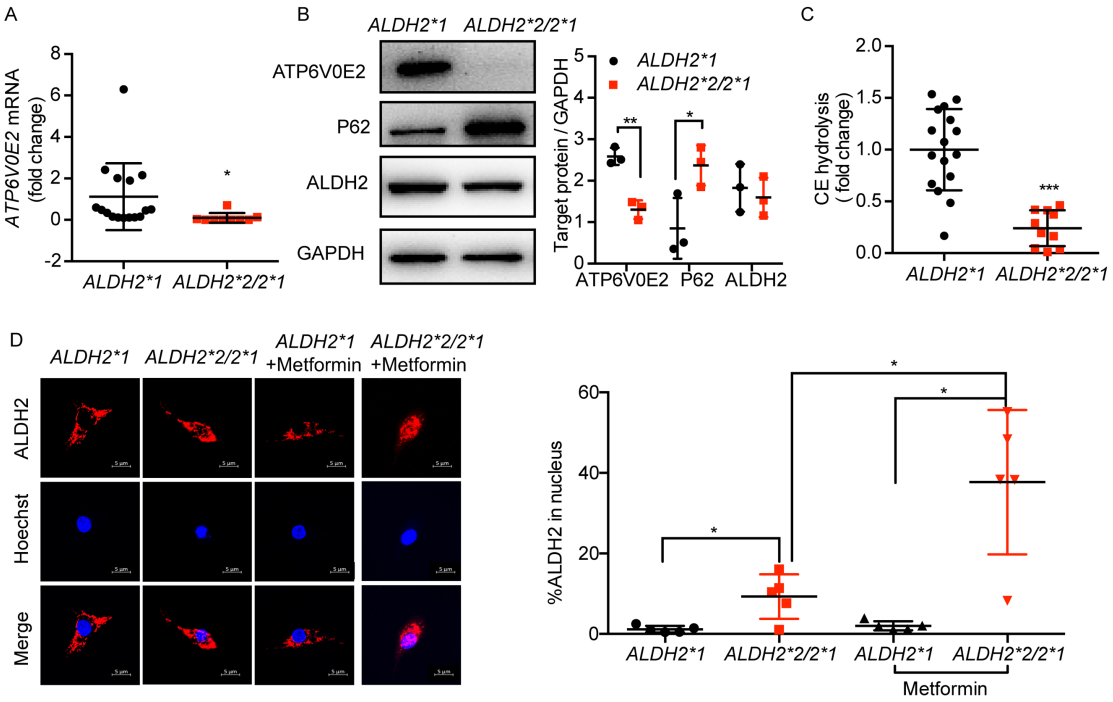

Figure 8. Human macrophages from subjects carrying ALDH2 rs671 SNP have increased foam cell formation caused by the downregulation of ATP6V0E2 and autophagy due to increased nuclear translocation of ALDH2.

A, macrophages from ALDH2*2/2*1 (n=10) have lower *ATP6V0E2* mRNA levels than those from *ALDH2*1* (n=16). **B,** ALDH2 rs671 mutant increased autophagy in human macrophages treated with oxLDL (n=3). **C,** ALDH2 rs671 mutant decreases CE hydrolysis in human macrophages (*ALDH2*1*, n=16; *ALDH2*2/2*1*, n=10). **D,** ALDH2 rs671 SNP increases ALDH2 translocation in human macrophages treated with Metformin (n=5). Statistical comparisons were made using 2-tailed Student's t test. All data represent mean ± SD.*P < 0.05, **P < 0.01, ***P < 0.001.

Figure 9

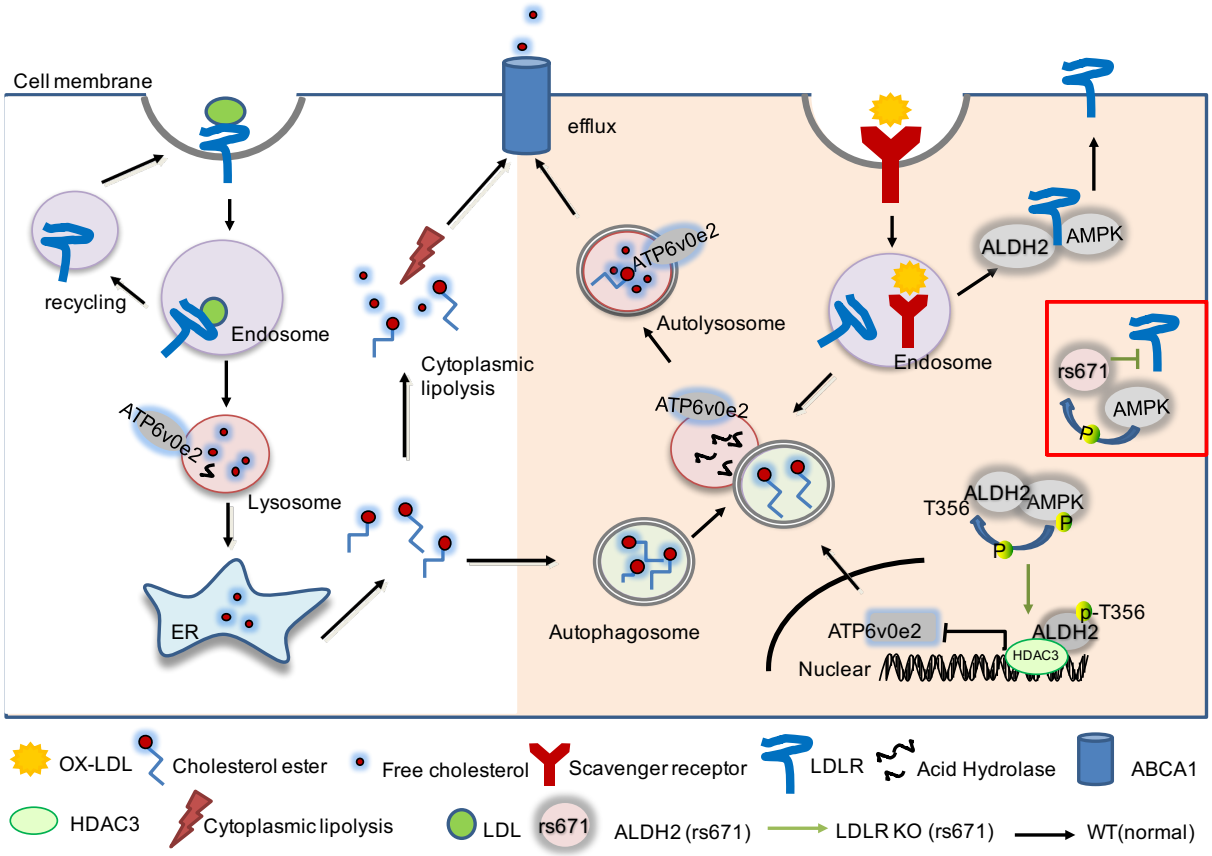

Figure 9. ALDH2 regulates macrophage foam cell formation through interacting with LDLR and AMPK: the translocation of AMPK phosphorylated ALDH2 to nucleus to regulate expression of ATP6V0E2, a critical protein for lysosomal function, endocytosis, and autophagy.